



HAL
open science

Reduced obesity, diabetes and steatosis upon cinnamon and grape pomace are associated with changes in gut microbiota and markers of gut barrier

Matthias van Hul, Lucie Geurts, Hubert Plovier, Céline Druart, Amandine Everard, Marcus Ståhlman, Moez Rhimi, Kleopatra Chira, Pierre Louis Teissedre, Nathalie M. Delzenne, et al.

► To cite this version:

Matthias van Hul, Lucie Geurts, Hubert Plovier, Céline Druart, Amandine Everard, et al.. Reduced obesity, diabetes and steatosis upon cinnamon and grape pomace are associated with changes in gut microbiota and markers of gut barrier. *AJP - Endocrinology and Metabolism*, 2018, 314 (4), pp.E334-E352. 10.1152/ajpendo.00107.2017 . hal-02626402

HAL Id: hal-02626402

<https://hal.inrae.fr/hal-02626402>

Submitted on 26 May 2020

HAL is a multi-disciplinary open access archive for the deposit and dissemination of scientific research documents, whether they are published or not. The documents may come from teaching and research institutions in France or abroad, or from public or private research centers.

L'archive ouverte pluridisciplinaire **HAL**, est destinée au dépôt et à la diffusion de documents scientifiques de niveau recherche, publiés ou non, émanant des établissements d'enseignement et de recherche français ou étrangers, des laboratoires publics ou privés.



Distributed under a Creative Commons Attribution 4.0 International License

1 **Reduced obesity, diabetes and steatosis upon cinnamon and grape pomace**
2 **are associated with changes in gut microbiota and markers of gut barrier**

3 Matthias Van Hul¹, Lucie Geurts¹, Hubert Plovier¹, Céline Druart¹, Amandine
4 Everard¹, Marcus Ståhlman², Moez Rhimi³, Kleopatra Chira,^{6,7} Pierre-Louis
5 Teissedre^{6,7}, Nathalie M. Delzenne¹, Emmanuelle Maguin³, Angèle Guilbot⁴,
6 Amandine Brochot^{4#}, Philippe Gérard^{#3}, Fredrik Bäckhed^{#2,5}, Patrice D. Cani^{1*}

7
8 ¹ Université catholique de Louvain, Louvain Drug Research Institute, WELBIO
9 (Walloon Excellence in Life sciences and BIOTEchnology), Metabolism and
10 Nutrition research group, Brussels, Belgium,

11 ² Wallenberg Laboratory, University of Gothenburg, Gothenburg, Sweden

12 ³ Micalis, INRA, AgroParisTech, Université Paris-Saclay, 78350, Jouy-en-Josas,
13 France.

14 ⁴ Groupe PiLeJe, 75015, Paris, France.

15 ⁵ Novo Nordisk Foundation Center for Basic Metabolic Research, Section for
16 Metabolic Receptology and Enteroendocrinology, Faculty of Health Sciences,
17 University of Copenhagen, Copenhagen, Denmark.

18 ⁶ Univ. Bordeaux, ISVV, EA 4577 Œnologie, F-33140 Villenave d'Ornon, France

19 ⁷ INRA, ISVV, USC 1366 Œnologie, F-33140 Villenave d'Ornon, France

20
21 # Equally contributed to this work

22
23 *Correspondence to: Patrice.cani@uclouvain.be
24 Prof. Patrice D. Cani, Université catholique de Louvain, LDRI, Metabolism and
25 Nutrition research group, Av. E. Mounier, 73 box B1.73.11, B-1200 Brussels,
26 Belgium. Phone: +32 2 764 73 97

27 **Running title:** Cinnamon and grape extracts shape microbiota and metabolism

28 **Abstract**

29 Increasing evidence suggests that polyphenols have a significant potential in the
30 prevention and treatment of risk factors associated with metabolic syndrome.
31 The objective of this study was to assess the metabolic outcomes of two
32 polyphenol-containing extracts from cinnamon bark (CBE) and grape pomace
33 (GPE) on C57BL/6J mice fed a high-fat diet (HFD) for 8 weeks.

34 Both CBE and GPE were able to decrease fat mass gain and adipose tissue
35 inflammation in mice fed a HFD without reducing food intake. This was
36 associated with reduced liver steatosis and lower plasma non-esterified fatty
37 acids levels. We also observed a beneficial effect on glucose homeostasis as
38 evidenced by an improved glucose tolerance and a lower insulin resistance
39 index.

40 These ameliorations of the overall metabolic profile were associated to a
41 significant impact on the microbial composition, which was more profound for
42 the GPE than for the CBE. At the genus level, *Peptococcus* were decreased in the
43 CBE group. In the GPE treated group, several key genera that have been
44 previously found to be linked with HFD, metabolic effects and gut barrier
45 integrity were affected: we observed a decrease of *Desulfovibrio*, *Lactococcus*,
46 whereas *Allobaculum* and *Roseburia* were increased.

47 In addition, the expression of several antimicrobial peptides and tight junction
48 proteins was increased in response to both CBE and GPE supplementation,
49 indicating an improvement of the gut barrier function.

50 Collectively, these data suggest that CBE and GPE can ameliorate the overall
51 metabolic profile of mice on a high-fat diet, partly by acting on the gut
52 microbiota.

53 Introduction

54 With more than one third of the adult population affected worldwide, obesity-
55 associated metabolic disorders have become a major global health challenge that
56 extends well beyond the developed world (1). Obesity is caused by a disparity
57 between energy intake and energy expenditure, although genetic and
58 environmental factors also influence this balance and modify metabolism (2).
59 Obesity is associated with an excess of (white) adipose tissue mass, insulin
60 resistance, liver fat accumulation, chronic pro-inflammatory state and major
61 health issues that include a plethora of comorbidities, such as type 2 diabetes,
62 cardiovascular diseases, hypertension, stroke, and certain types of cancer (3).
63 Weight-reducing programs that recommend switching to a healthier lifestyle
64 with reduced caloric intake and increased physical activity, although efficient,
65 are difficult to maintain in the long term and therefore often remain unsuccessful
66 (4). Unfortunately, available drugs are of limited efficacy and are associated with
67 side effects (5). Plant extracts may represent an additional option in the support
68 of weight management strategies (6).

69 Among these, polyphenols, a large family of compounds identified in plants, have
70 attracted great interest because of their beneficial health effects (7). These
71 effects are often attributed to their ability to relieve oxidative stress-induced
72 tissue damage associated with chronic diseases via their antioxidant activity and
73 free radical scavenging capacities. Interestingly, some polyphenols were shown
74 to have anti-inflammatory and antimicrobial properties, thereby influencing the
75 host gut microbiota, and eventually the inflammatory and metabolic status (8-
76 12). In addition, we and others have demonstrated that the gut microbiota

77 contributes to the development of the metabolic disorders associated with
78 obesity by modulating appetite (13, 14), energy harvest and absorption (14-16),
79 gut motility, intestinal barrier function, inflammation (17, 18), glucose and lipid
80 metabolism, as well as hepatic and adipose tissue fat storage (19). It was also
81 reported that diets containing high fat levels diminish intestinal microbial
82 diversity, often at the expense of more beneficial bacteria (20).

83 The aim of the present study was to determine the effects of two extracts of
84 plants, cinnamon and grape pomace, known to be rich in polyphenols, in a mouse
85 model of diet-induced obesity. Anti-diabetic and anti-inflammatory properties of
86 cinnamon were reported in experimental studies (21-26) and the beneficial
87 effects of grapes and grape by-products were documented in different aspects of
88 the metabolic syndrome including dyslipidaemia, diabetes, hypertension, and
89 obesity (27-29). However, only few studies have explored the impact of dietary
90 polyphenols on the gut microbiota and intestinal barrier functions (28, 30-32),
91 and many aspects of this interaction remain largely unknown. This assessment
92 was therefore one of the main objectives of this study.

93

94 **Materials and Methods**

95 **Extracts**

96 The cinnamon bark extract (CBE), ChalCinn[®], (3inature, Saint-Bonnet-de-
97 Rochefort, France) was extracted from *Cinnamomum cassia*, rich in polyphenol
98 type-A polymers (oligomeric proanthocyanidins)(21, 33).

99 The grape (*Vitis vinifera L.*) pomace extract (GPE) was supplied by 3iNature and
100 sourced from Alicante from red wine cultivar in the Rhône valley. Grape pomace
101 is a wine by-product that is characterized by high contents of phenolic

102 compounds due to an incomplete extraction during the winemaking process. It is
103 a mixture of grape skins and seeds in near-equivalent amounts together with a
104 small amount of stems (<6 %). The main polyphenols of grape pomace are
105 anthocyanins, hydroxycinnamic acids, flavanols and flavanol glycosides (34).
106 Extraction was performed with ethanol/water (30:70 v/v) at 85 °C and the
107 extract was concentrated and vacuum-dried on non-extracted grape pomace.
108 The final product thus consisted of Alicante grape pomace enriched with its own
109 polyphenols.

110

111 **Reagents and Standards**

112 Deionized water was purified with a Milli-Q water system (Millipore, Bedford,
113 MA, USA). HPLC grade acetonitrile, ethyl acetate, chloroform, methanol, ethanol
114 and acetone purchased from Scharlau (Sentmenat, Barcelona, Spain). The
115 following chemicals were obtained from Sigma Aldrich (St. Louis, MO, USA): (+)-
116 catechin, (-)-epicatechin, B1 [(-)-epicatechin-(4 β -8)-(+)-catechin], procyanidin
117 dimer B2 [(-)-epicatechin-(4 β -8)-(-)-epicatechin], cyanidin-3-O-glucoside
118 chloride, delphinidin-3-O-glucoside chloride, malvidin-3-O-glucoside chloride,
119 peonidin-3-O-glucoside chloride, gallic acid.

120 The Laboratory of Organic Chemistry and Organometallic (Université Bordeaux
121 1) synthesized procyanidins dimers B3 [(+)-catechin-(4 α -8)-(+)-catechin], B4
122 [(+)-catechin-(4 α -8)-(-)-epicatechin] and a trimer (C1) [(+)-catechin-(4 β -8)-(+)-
123 catechin-(4 β -8)-(-)-epicatechin] (Tarascou et al., 2006).

124

125

126 **Grape pomace extract analysis**

127 **Tannins Extraction**

128 GPE (1 gr of dry matter) was solubilized in water/ethanol (250 mL, 95:5, v/v)
129 and partitioned three times with chloroform (250 mL) to remove lipophilic
130 material. The aqueous phase was then extracted three times with ethyl acetate
131 (250 mL) to obtain two distinctive fractions: a low molecular weight procyanidin
132 fraction (monomeric/oligomeric tannins) in the organic phase and a high weight
133 procyanidin fraction (polymeric tannins) in the aqueous phase. These two
134 fractions were concentrated and lyophilized.

135

136 **Anthocyanins Extraction**

137 Anthocyanin extraction was adapted from the method of Sriram et al. (1999).
138 GPE (1 g) was extracted four times with acidified methanol (40 mL, 0.1% HCl
139 12N) successively for 4 h, 12 h, 4 h and 12 h. The centrifugal supernatants were
140 combined and evaporated in vacuo at 30 °C to remove methanol; the residue was
141 dissolved in water and lyophilized to obtain an anthocyanin-rich powder.

142

143 **Total Phenolics and Tannins, Anthocyanins**

144 Total polyphenol contents (TPC) were determined in GPE and cinnamon bark
145 extract (CBE). Tannin and anthocyanin contents were determined only in GPE.
146 Crude extracts were solubilized in water/ethanol (90:10, v/v; pH 3.5 with
147 tartaric acid) at appropriate concentrations. TPC was determined by the Folin-
148 Ciocalteu assay [Singleton et al., 1965] and the data expressed as mg of gallic acid
149 equivalents (GAE) per g dry weight. Total tannin content was measured by acidic
150 hydrolysis using the method of Ribereau-Gayon and Stonestreet [Ribéreau et al.,

151 1966]. Anthocyanin content was determined by the SO₂ bleaching procedure
152 [Ribéreau et al., 1965].

153

154 **HPLC Analysis of Anthocyanins in GPE**

155 GPE was dissolved in water/methanol solution (50:50, v/v) at a concentration of
156 10 mg/mL prior to UPLC-UV analyses using a Thermo-Accela HPLC system
157 (Thermo-Fisher, San Jose, CA, USA) composed of a PDA detector, an autosampler
158 and a quaternary 600 series pump system controlled by an Xcalibur data system.

159 Separation was performed on a C18 Kinetex column (100 mm × 2.1 mm, 1.7 μm).

160 The injected volume was 2 μL. The mobile phase pumped at 200 μL/min

161 comprised a 20 min, 7%–26% gradient of acetonitrile in water with both

162 solvents containing 5% formic acid. Eluting peaks were monitored at 520 nm.

163 Identification of main peaks was performed by comparison to external

164 standards (Anthocyanins monoglucosides (cyanidin-3-O-glucoside, delphinidin-3-

165 O-glucoside, paeonidin-3-O-glucoside, malvidin-3-O-glucoside, petunidin-3-O-

166 glucoside), acylated anthocyanins (paeonidin-3-O-glucoside, malvidin-3-O-

167 glucoside) and coumaroylated (paeonidin-3-O-glucoside, malvidin-3-O-

168 glucoside). The data was expressed as Malvidin-3-O-glucoside equivalent/g dry

169 weight GPE. (Ky et al., 2014).

170

171 **Determination of Individual Tannins in GPE by HPLC Analysis**

172 GPE extract was solubilized in a methanol/water solution (50:50, v/v) at

173 appropriate concentrations and analyses of monomeric/oligomeric tannins

174 (catechin, epicatechin, dimers B1, B2, B3, B4 ; Trimer C2) were carried out

175 according to the method of Silva et al. [Silva et al, 2012]. The data was expressed
176 as catechin equivalent/g dry weight GPE.

177

178 **Determination of Mean Degree of Polymerization (mDP) in GPE**

179 The proanthocyanidin mean degree of polymerization (mDP) was determined
180 for GPE in monomeric/oligomeric and polymeric tannin fractions by the means
181 of phloroglucinolysis [Drinkine et al., 2007]. Analyses were carried out using the
182 same method as described by Lorrain et al. [Lorrain et al., 2011].

183 The oligomeric and polymeric proanthocyanidins were depolymerised in the
184 presence of a nucleophilic agent phloroglucinol in an acidic medium. Reversed-
185 phase HPLC analysis of the products formed allows determination of the
186 structural composition of proanthocyanidins, which are characterised by the
187 nature of their constitutive extension units (released as flavan-3-ols
188 phloroglucinol adducts) and terminal units (released as flavan-3-ols). To
189 calculate the apparent mDP, the sum of all subunits (flavan-3-ol monomer and
190 phloroglucinol adducts, in mols) was divided by the sum of all flavan-3-ol
191 monomers (in mols). GPE sample was analysed with a Surveyor series
192 instrument (Thermo-Finnigan, Les Ullis, France) equipped with a 100 x 4.6 mm
193 i.d., 3.5 μ m X-Terra reversed-phase C18 column (Waters) thermostated at
194 25°C. Detection was carried out at 280 nm using a Finnigan Surveyor PDA Plus
195 detector. The mass detection was carried out using a Finnigan LCQ DECA XP MAX
196 mass spectrometer with an ESI interface, performed in positive mode with the
197 following parameters: capillary temperature 325 °C, capillary voltage 4 V,
198 nebulizer gas flow 1.75 L/min, desolvation gas flow 1 L/min, and spray voltage 5
199 kV. The solvents used were solvent A: H₂O/AcOH (99:1 v/v), and B: MeOH. The

200 gradient consisted of 5% B during 25 min, linear gradient 5%–20% B in 20 min,
201 then 20%–32% B in 15 min, finally 32%–100% B in 2 min. The column was
202 washed with 100% B for 5 min and then stabilized with the initial conditions for
203 10 min. The injection volume was 20 µL. The flow rate was 1 mL/min.

204

205 **Cinnamon bark extract analysis**

206 **Total proanthocyanidins**

207 In CBE, total proanthocyanidin content (PAC) was determined in EP using the
208 BL-DMAC method as previously described (Lee et al., 2009) and quantified as A-
209 type proanthocyanidin equivalents.

210

211 **Determination of essential oil in CBE**

212 CBE was ground and submitted to steam distillation (20,0 g of dried material) for
213 8 h, using a Clevenger-type apparatus without hexane at a rate of 3-4 ml/min,
214 according European Pharmacopoeia. The volatile distillates were analyzed by
215 GC-MS. The ratio of CBE and water (acidified by 2 ml HCL 37% m/m) was 1:10.
216 The essential oils were stored in amber vials at 4°C until analysis. The yield oil
217 were kept frozen at temperature -20°C up to their utilization.

218 The essential oil were analysed on a Agilent gas chromatograph Model 7890,
219 coupled to a Agilent MS model 5975 coupled to a computer equipped with
220 Chemstation, equipped with a DB5 MS column (40m X 0.18mm, 0.18µm),
221 programming from 50°C (5 min) to 300°C at 5°C/min, 5 min hold. Helium as
222 carrier gas (1.0 ml/min); injection in split mode (1:80) ; injector, 280°C. The MS
223 working in electron impact mode at 70 eV; electron multiplier, 1900 V; ion
224 source temperature, 230°C ; mass spectra data were acquired in the scan mode

225 in m/z range 33-450. The essential oil is diluted in acetone: 1/100. The essential
226 oil were analysed on a Agilent gas chromatograph Model 7890, equipped with a
227 DB5 MS column (40m X 0,18mm, 0.18 μm), programming from 50°C (5 min) to
228 300°C at 5°C/min, 5 min hold. Helium as carrier gas (1.0 ml/min); injection in
229 split mode (1:80); injector and detector temperature, 280 and 300°C
230 respectively. The essential oil is diluted in acetone: 1/100.

231 Components were identified by both GC retention times and by comparison of
232 their mass with those present in the computer data bank and published spectra.
233 Quantification was performed by area percent, FID-response factor = 1.

234

235 **Determination of coumarin content in CBE**

236 About 3.0 g (accurately weighed to 0,0001 g) of powdered whole plant was
237 extracted using 150 ml methanol R as solvent under reflux during 30 min. After
238 filtration, the filtrate was adjusted to 250,0 ml with the same solvent. The sample
239 were filtered using 0,45 μm membrane filters (Millipore). Quantification of the
240 constituent coumarin was carried out from the calibration curves of the HPLC
241 chromatograms using authentic compounds. Coumarin (> 98%, HPLC)
242 purchased from Sigma (St. Louis, MO, USA) was used as an external standard.

243 The coumarin content was determined according to reported methods [1] by an
244 HPLC apparatus (Hitachi) consisting of a quaternary pump, a autosampler, and a
245 Photodiode Array Detector (PDA). Separation was carried with a C18 column
246 (4.6 mm x 250 mm) Purospher Star VWR. The column temperature was
247 maintained at 25°C and the mobile phase flow rate at 1.5 ml/min. The mobile
248 phase consisted of HPLC grade solvent Acetonitrile R and 5 g/L Phosphoric acid

249 (22:78 V/V). Coumarin content was quantified at 275 nm against the respective
250 external standard.

251

252 **Mice**

253 Nine-week-old male C57BL/6J mice (Janvier, Le Genest-Saint-Isle, France) were
254 housed in pairs in specific pathogen free conditions and in controlled
255 environment (room temperature of 23 ± 2 °C, 12 h daylight cycle) with free
256 access to food and water. After an acclimatization period of one week, mice were
257 randomly assigned to one of four dietary conditions (n = 14 per group). The
258 different diets were as follow: control diet (CT) (10 kcal% fat, D12450Ji,
259 Research Diet, New Brunswick, NJ, USA), high-fat diet (HFD) (60 kcal% fat,
260 D12492i Research Diet), high-fat diet supplemented with 2 g cinnamon bark
261 extract/kg (HFD-CBE) or a high-fat diet supplemented with 8.2 g grape pomace
262 extract/kg (HFD-GPE) during 8 weeks. Body weight, food and water intake were
263 recorded weekly. Body composition (lean and fat mass) was assessed by using
264 7.5MHz time domain-nuclear magnetic resonance (TD-NMR) (LF50 Minispec,
265 Bruker, Rheinstetten, Germany). In the final week of the experiment, feces were
266 collected for each mouse and energy content was measured by calorimetric
267 bomb analysis (Mouse Clinical Institute, Illkirch, France).

268 All mouse experiments were approved by and performed in accordance with the
269 guidelines of the local ethics committee. Housing conditions were specified by
270 the Belgian Law of May 29, 2013, regarding the protection of laboratory animals
271 (agreement number LA1230314).

272

273

274 **Oral glucose tolerance test (OGTT)**

275 After 7 weeks of treatment, an oral glucose tolerance test (OGTT) was performed
276 as previously described (35). Briefly, 6h-fasted mice were given an oral glucose
277 load (2 g glucose per kg body weight) and blood glucose levels were measured at
278 different time points: 30 min before and 15, 30, 60, 90 and 120 min after oral
279 glucose load. Blood glucose was measured with a standard glucose meter (Accu
280 Check, Roche, Basel, Switzerland) on blood samples collected from the tip of the
281 tail vein.

282

283 **Insulin resistance index**

284 Plasma insulin concentration was determined using an ELISA kit (Mercodia,
285 Uppsala, Sweden) according to the manufacturer's instructions. Insulin
286 resistance index was determined by multiplying the area under the curve of both
287 blood glucose (-30 to 120 min) and plasma insulin (-30 and 15 min) obtained
288 following the oral glucose tolerance test (36). Glucose-induced insulin secretion
289 was calculated as the difference between plasma insulin levels 30 min before and
290 15 min after oral glucose load.

291

292 **Tissue sampling**

293 At the end of the treatment period (week 8), 9 animals from each group were
294 anesthetized with isoflurane (Forene, Abbott, Queenborough, Kent, England) and
295 blood was sampled from the portal and cava veins. After exsanguination, mice
296 were killed by cervical dislocation. Subcutaneous adipose tissue depots,
297 intestines, muscles and liver were precisely dissected, weighed and immediately
298 immersed in liquid nitrogen followed by storage at -80°C for further analysis.

299 **Indirect calorimetry experiments**

300 The remaining mice ($n = 5$ per group) were housed individually in specialized
301 metabolic chambers (Phenomaster, TSE Systems GmbH, Bad Homburg,
302 Germany) to measure whole energy expenditure, oxygen (O_2) consumption and
303 carbon dioxide (CO_2) production, respiratory exchange ratio (RER, calculated as
304 vCO_2/vO_2), food intake and spontaneous locomotor activity (36, 37). Activity was
305 recorded using an infrared light beam-based locomotion monitoring system
306 (expressed as counts per hour). Mice were allowed 48 h acclimatization before
307 experimental measurements. After six days of measurements, mice were killed
308 and tissues were sampled as described above.

309

310 **Histological analyses**

311 Subcutaneous adipose tissue depots were fixed in 4% paraformaldehyde for 24
312 hours at room temperature. Samples were then immersed in ethanol 100 % for
313 24 hours prior to processing for paraffin embedding.

314 To determine the adipocyte tissue diameter, paraffin sections of 8 μm were
315 stained with hematoxylin and eosin.

316 Macrophage infiltration in the adipose tissue was assessed by staining them with
317 a MAC-2/galectin-3 antibody (CL8942AP, Cedarlane Laboratories, Burlington,
318 Ontario, Canada) diluted 1:500 in blocking buffer overnight, and was detected
319 with an anti-rat igG antibody (AI-4001, Vector Laboratories, Inc., Burlingame,
320 California, USA) (10 mg/ml). Immune complexes were detected by the Dako
321 Envision kit (Agilent Technologies, Santa Clara, California, USA) according to the
322 manufacturer's instructions, and briefly counterstained with haematoxylin.

323 Hepatic lipid content was visualized by using Oil red O staining.

324 All analyses were performed in a blinded manner by the investigator and
325 quantified using ImageJ software (Version 1.50a, National Institutes of Health,
326 Bethesda, Maryland, USA). At least five high-magnification fields were selected at
327 random for each mouse. Images were obtained using a SCN400 slide scanner and
328 Digital Image Hub software (Leica Biosystems, Wetzlar, Germany).

329

330 **RNA preparation and Real-time qPCR analysis**

331 Total RNA was prepared from tissues using TriPure reagent (Roche).
332 Quantification and integrity analysis of total RNA were performed by analyzing
333 1 µl of each sample in an Agilent 2100 Bioanalyzer (Agilent RNA 6000 Nano Kit,
334 Agilent, Santa Clara, California, USA). cDNA was prepared by reverse
335 transcription of 1 µg total RNA using a Reverse Transcription System kit
336 (Promega, Madison, Wisconsin, USA). Real-time PCR was performed with the
337 CFX96 real-time PCR system and CFX Manager 3.1 software (Bio-Rad, Hercules,
338 California, USA) using Mesa Fast qPCR (Eurogentec, Liège, Belgium) for detection
339 according to the manufacturer's instructions. RPL19 was chosen as the
340 housekeeping gene. All samples were performed in duplicate, and data were
341 analyzed according to the $2^{-\Delta\Delta CT}$ method. The identity and purity of the amplified
342 product were assessed by melting curve analysis at the end of amplification. The
343 primer sequences for the targeted mouse genes are presented in Table 1.

344

345 **Biochemical analyses**

346 Plasma adipokines (leptin, resistin) and inflammatory markers (IL1b, IFNg,
347 MCP1, MIP1a, PAI1) were detected by using a Bio-Plex Milliplex kit (Millipore,
348 Billerica, Massachusetts, USA) and their concentrations were measured by using

349 Luminex technology (Bio-Rad Bioplex; Bio-Rad) following the manufacturer's
350 instructions.

351 Plasma non-esterified fatty acids, cholesterol and triglyceride concentrations
352 were measured using kits coupling an enzymatic reaction with
353 spectrophotometric detection of the reaction end-products (Diasys Diagnostic
354 and Systems, Holzheim, Germany) according to the manufacturer's instructions.

355 Total lipids were measured in the liver tissue after extraction in CHCl₃:MeOH
356 according to Folch et al. (38) and adapted as follows: Briefly, 100 mg of liver
357 tissue was homogenized in 2 ml of CHCl₃:MeOH (2:1) using a Tissue Lyser
358 followed by an ultrasonic homogenizer. 400 µl of 0.9% NaCl solution was added
359 and lipids were then extracted by vigorous shaking. After centrifugation, the
360 lipidic phase was recovered in glass tubes and dried under a stream of N₂. Glass
361 tubes were weighed before and after lipid extraction to quantify total lipid
362 content. The dried residue was solubilized in 1.5 to 3 ml isopropanol depending
363 on the lipid content.

364

365 **Short chain fatty acid (SCFA) measurements**

366 Short-chain fatty acids in cecal samples were analyzed by gas-liquid
367 chromatography as described previously (39).

368

369 **Bile Acids (BA) measurements**

370 The extraction and analysis of bile acids were performed according to a previous
371 work (40). Briefly, bile acids from portal vein plasma were extracted by protein
372 precipitation with 10 volumes of IS-containing methanol. After the samples were
373 vortexed and centrifuged, the supernatant was diluted 50 times in

374 methanol:water (1:1). Bile acids from cecum (15-100 mg in 2 ml polypropylene
375 tubes filled with ceramic beads) were extracted in 500µl IS-containing methanol
376 using a TissueLyser II instrument (Retsch, Haan, Germany). The supernatant was
377 diluted 50 times in methanol:water (1:1). Separation was performed using water
378 and acetonitrile on a Kinetex C18 column (2.1 ×100 mm with 1.7 µm particles;
379 Phenomenex, Torrance, California, USA). Detection was performed using a
380 QTRAP 5500 instrument (AB Sciex, Toronto, Canada) with MRM in negative
381 mode.

382

383 **Gut microbiota analysis**

384 The V3-V4 region was amplified from purified DNA with the primers F343
385 (CTTTCCTACACGACGCTCTTCCGATCTACGGRAGGCAGCAG) and R784
386 (GGAGTTCAGACGTGTGCTCTTCCGATCTTACCAGGGTATCTAATCCT) using 30
387 amplification cycles with an annealing temperature of 65°C. The amplicon
388 lengths were about 510 bp (the exact length varies depending on the species).
389 Because MiSeq sequencing enables paired 250-bp reads, the ends of each read
390 overlap and can be stitched together to generate extremely high-quality, full-
391 length reads covering the entire V3-V4 region. Single multiplexing was
392 performed using a home-made 6 bp index, which was added to the R784 primer
393 during a second PCR with 12 cycles using the forward primer
394 (AATGATACGGCGACCACCGAGATCTACTCTTTCCTACACGAC) and the
395 modified reverse primer (CAAGCAGAAGACGGCATACGAGAT-index-
396 GTGACTGGAGTTCAGACGTGT). The resulting PCR products were purified and
397 loaded onto the Illumina MiSeq cartridge according to the manufacturer
398 instructions. The quality of the run was checked internally using PhiX, and for

399 further analysis, each pair-end sequence was assigned to its sample using the
400 previously integrated index.

401

402 **Bioinformatics analysis**

403 Sequences were trimmed for adaptors and assembled with Flash1.6.2 (41). PCR
404 primers were removed and sequences with sequencing errors in the primers
405 were excluded (Mothur) (42). For each sample, 12000 reads were randomly
406 selected for each sample. Chimera were removed with UCHIME (43) and Mothur
407 (42) softwares. Reads were clustered into Operational Taxonomic Units (OTUs)
408 at the 97% identity level using Esprit-tree (44). A reference sequence was picked
409 for each OTU and assigned it at different taxonomic levels (from phylum to
410 species) using the Greengenes database (release 13-5) (45) and the RDP
411 classifier (46).

412

413 **Statistical analysis**

414 Mouse data are expressed as the mean \pm SEM. Differences between groups were
415 assessed using non-parametric Kruskal–Wallis one-way analysis of variance
416 (ANOVA), followed by the Dunn’s multiple comparison test. Variance was
417 compared using a Bartlett’s test. If variances were significantly different between
418 groups, values were normalized by Log-transformation before proceeding to the
419 analysis. When only two groups were compared, a non-parametric Mann-
420 Whitney test was used. Regimen and treatment effects on community
421 compositions were assessed using permutational multivariate analysis of
422 variances (PERMANOVA) after rarefaction of all communities to even sampling
423 depths. The abundances of all families were computed by agglomerating the

424 OTUs assigned to those families. For each such family, Mann-Whitney test with
425 BH correction (47) were performed to detect the combinations (treatment) that
426 were significantly different in terms of abundance. The same procedure was
427 applied for each genus and for each OTUs. All analyses were done using R (R
428 Core Team, 2015, R Foundation for Statistical Computing, Vienna, Austria)
429 A two-way ANOVA analysis with a Bonferonni post-hoc test on repeated
430 measurements was performed for the evolution of glycaemia and insulinemia
431 during the OGTT. For all analyses and for each group, any exclusion decision was
432 supported by the use of the Grubbs test for outlier detection.

433 Results

434 **Polyphenol content and profile of grape and cinnamon extracts**

435 GPE contained 82.663 ± 2.534 mg/g total phenolics as gallic acid equivalents
436 (GAE). Total anthocyanin and tannin contents of the GPE fraction were $43.969 \pm$
437 3.497 (as cyanidin-3-O-glucoside equivalent) and 26.006 ± 1.066 (as procyanidin
438 B2 equivalent), respectively, (Table 2). Individual anthocyanin analysis revealed
439 that the most abundant anthocyanins present in GPE were malvidin-3-O-
440 glucoside (21.594 ± 0.213 mg/g), peonidin-3-O-glucoside (8.687 ± 0.258 mg/g)
441 and malvidin-3-O-(6''-p-coumaryl-glucoside) (4.624 ± 0.012 mg/g) (Table 2).
442 The mean degree of polymerization of the proanthocyanidins in the GPE fraction
443 was 4.2 ± 0.025 (data not shown).

444 CBE contained 79 mg/g of total phenolics as GAE. Proanthocyanidin A content
445 was 90 mg/g. Coumarin and cinnamaldehyde represented 9 mg/g and 1.8 mg/g
446 respectively.

447

448 **Effects on body weight, body composition, adipose tissues and adipokines**

449 Body weight gain and fat mass gain were both significantly greater in all high-fat
450 diet treated groups (HFD, HFD-CBE, HFD-GPE) than in mice fed the control diet
451 (CT) (Fig 1A, B). Compared to the HFD-group, HFD-GPE ($p = 0.03$, 2-way
452 repeated measurements ANOVA) and -CBE groups (trend, $p = 0.1$) had a lower
453 fat mass gain during the last 4 week of follow-up (Fig 1B, E, F) but no significant
454 difference in body weight and lean mass gain were observed in the extract-
455 treated groups (Fig 1A-F).

456 Brown and White adipose tissue depots were consistently smaller in the extract-
457 treated groups compared to the HFD group, but there was no statistical
458 difference (Fig 1G-I). These findings were mirrored by a trend in reduced leptin
459 plasma levels in the HFD-GPE group ($p = 0.08$ versus HFD, Mann-Whitney test)
460 (Fig 1J).

461 The weights of liver, spleen and different muscles were not affected by the
462 different diets (data not shown).

463

464 **Effects on glucose homeostasis**

465 Both CBE and GPE treatments significantly improved glucose tolerance, as
466 evidenced by a lower blood glucose profile compared to the untreated HFD-fed
467 group (Fig 2A). The effect was stronger for the HFD-CBE group as evidenced by
468 the significantly reduced area under the curve (Fig 2B).

469 Mice fed a HFD were hyperinsulinemic in the fasted state, as they exhibited more
470 than two-fold higher levels of plasma insulin as compared to control mice (Fig
471 2C). Mice from the HFD-GPE group produced somewhat less insulin in response
472 to oral glucose administration compared to the HFD and HFD-CBE mice without
473 reaching statistical significance (Fig 2C) ($p = 0.07$ versus HFD, Mann-Whitney
474 test). This result was corroborated by a decreasing trend for glucose-induced
475 insulin secretion compared to the HFD and HFD-CBE groups ($p = 0.08$ versus
476 HFD, non-parametric Mann-Whitney test)(Fig 2D) and a significant improvement
477 of the insulin resistance index (Fig 2E) in the HFD-GPE treated group. This was in
478 accordance with a smaller adipocyte size (Fig 2F-G) and a trend in lower
479 circulating resistin levels (Fig 2H), factors that have previously been associated
480 with insulin resistance (37). For the HFD-CBE group no difference in glucose-

481 induced insulin secretion could be observed but there was a trend towards an
482 improvement of the insulin resistance index compared to the HFD group ($p =$
483 0.06 versus HFD, Mann-Whitney test)(Fig 2E).

484

485 **Effects on energy homeostasis**

486 The reduced fat mass gain observed in HFD-GPE mice could not be explained by
487 any difference in energy intake (Fig 3A). On the contrary, there was a trend
488 towards a higher mean calorie intake in HFD-GPE mice ($p = 0.08$ versus HFD,
489 Mann-Whitney test). HFD-GPE mice also had a significantly increased amount of
490 feces excreted compared to the other HFD groups (Fig 3B). In addition, bomb
491 calorimetric analysis of the different groups revealed a higher energy content in
492 the fecal material of mice supplemented with cinnamon or grape extract (Fig 3C),
493 resulting in higher daily energy excretion in both groups, as compared to HFD
494 (Fig 3D). There was no difference when expressing this as percentage of the food
495 intake (Fig3E).

496 The basal energy expenditure, which can also affect energy balance, was
497 calculated by measuring the O_2 consumption and the CO_2 production for each
498 mouse (not shown). After correction for the individual lean masses, the analysis
499 revealed a mean increase in energy expenditure for the HFD, HFD-CBE and HFD-
500 GPE groups, as compared to the CT group, without any effect of dietary
501 supplementation (Fig 3F-G). In addition, body temperatures were not different
502 between all four groups (Fig 3H). The respiratory exchange rate (RER) showed a
503 clear metabolic shift from carbohydrate to lipid oxidation in the three HFD
504 treated groups as compared to CT mice (Fig 3I).

505 Spontaneous physical activity (monitored by continuously counting the number
506 of times a mouse crossed the different light beams in the metabolic cages) was
507 increased in HFD-GPE mice in comparison with HFD mice ($p = 0.02$ versus HFD,
508 2-way repeated measurement ANOVA) (Fig 3J), whereas this effect was less
509 pronounced in HFD-CBE mice ($p = 0.18$).

510

511 **Effects on nutrients absorption**

512 To investigate the mechanism associated with reduced energy harvest, we
513 measured different nutrient transporters in the proximal part of the intestines
514 (jejunum) (Fig3K). Glucose transporters (Slc5a1/SGLT1, Slc2a2/GLUT2) were
515 slightly lower in the high-fat fed group, whereas FABP1/LFABP and CD36, fatty
516 acid binding proteins, are higher, confirming the switch from glucose
517 consumption to lipid oxidation. Both CBE and GPE slightly increased SGLT1, but
518 only GPE increased GLUT2 as well. LFABP was somewhat decreased by the GPE,
519 as was CD36 by CBE. However, these changes were too subtle to achieve
520 statistical significance.

521

522 **Effects on whole-body and hepatic lipid metabolism**

523 The management of dyslipidemia is a key element in the prevention of
524 cardiovascular diseases in obese and diabetic patients. Therefore, we performed
525 an analysis of circulating and liver lipids. Interestingly, circulating non-esterified
526 fatty acids levels (NEFAs) were higher in the HFD group than in the control
527 group and were normalized in the CBE and GPE treated groups although without
528 reaching significance ($p = 0.06$ and 0.08 versus HFD respectively, Mann-Whitney

529 test). Cholesterol plasma levels were increased in all HFD-treated groups,
530 whereas circulating triglycerides were similar between groups (Fig 4A).
531 In the liver, HFD increased the total lipid content by about 40%. Interestingly,
532 treatment with GPE completely blunted this effect (Fig 4B). This was reflected by
533 a significant normalization of liver triglyceride levels and a similar trend for
534 cholesterol. In the HFD-CBE group, a trend for normalization was also observed
535 for total lipid content and triglycerides, while cholesterol levels remained
536 unaffected ($p = 0.06$ versus CT, $p = 0.6$ versus HFD, Mann-Whitney test). This
537 finding was confirmed by the histological analysis that revealed significantly
538 increased hepatic lipid depots in HFD mice, and smaller lipid droplets in the
539 HFD-CBE and HFD-GPE mice (Fig 4C).

540

541 **Effects on adipose tissue and systemic inflammation**

542 Diabetes and insulin resistance being frequently associated with adipose tissue
543 inflammation (17, 48, 49), we measured various macrophage infiltration
544 markers in the subcutaneous (SAT) and visceral adipose tissue (VAT) using qPCR
545 analysis (Fig 5A and 5B, respectively). Integrin alpha X (ITGAX/CD11c),
546 lipopolysaccharide binding protein (LBP) and monocyte chemoattractant
547 protein-1 (MCP1) were upregulated by HFD and were reduced by GPE in both
548 adipose tissues. CBE supplementation decreased CD11c and LBP, but not MCP1.
549 Two other macrophage markers, F4/80 and CD68, were not differently
550 expressed in any group (Fig 5A).

551 Histological analysis of the SAT stained with MAC2/Galectin-3, a marker of
552 activated macrophages, showed a 2.5-fold higher number of macrophages in the
553 HFD mice than in CT mice (Fig 5B), whereas this accumulation of macrophages

554 was markedly decreased in the HFD-CBE and HFD-GPE groups compared to the
555 HFD group, although without reaching significance (Fig 5B).

556 To evaluate systemic inflammation, we measured circulating inflammatory
557 markers in plasma (Fig 5D). We did not find a marked HFD effect for any of the
558 markers, indicating that although there is a tissue inflammatory tone, they have
559 not yet reached systemic inflammation. However, the GPE tended to be
560 systematically lower than the other groups, especially for IFN γ ($p = 0,02$ versus
561 HFD, Mann-Whitney test).

562

563 **Effects on gut microbiota**

564 We and others have previously linked the gut microbiota with low-grade
565 inflammation and metabolic disorders associated with HFD feeding (17, 50-52).

566 The composition of the gut microbiota of mice that received HFD was
567 significantly changed compared to those fed with CT diet, with an enrichment in
568 Firmicutes and a decrease in Bacteroidetes (Fig 6A).

569 At the phylum level, no clear differences were observed in HFD-CBE mice when

570 compared to HFD. GPE treatment, however, increased the abundance of

571 Bacteroidetes at the expense of the Proteobacteria (Fig 6A). As observed in the

572 principal coordinates analysis (PCoA), HFD feeding caused a shift in microbiota

573 composition along the axis 1, explaining more than 57% of the difference

574 observed (Fig 6C). Conversely, most mice from the HFD-CBE and HFD-GPE

575 groups were separated from the untreated HFD-fed mice according to the axis 2.

576 At the operational taxonomic units (OTUs) level, this shift was modest in the

577 HFD-CBE group but more profound in the HFD-GPE group (Fig 6B). More

578 specifically, the abundance of 11 OTUs was significantly different in HFD-CBE

579 mice compared with HFD mice. In HFD-GPE mice, 53 OTUs were significantly
580 modified (Fig 6B). Interestingly, the gut microbiota from extract-treated mice
581 differed from that of the HFD mice but also from that of the CT mice, suggesting
582 that polyphenols may have specific effects on the gut microbiota (Fig 6D).

583 At the family level, CBE supplementation significantly reduced the levels of
584 *Peptococcaceae* (classified within the Firmicutes phylum) when compared to the
585 HFD mice (Fig 6D, E). Supplementation with GPE reduced the levels of
586 *Desulfovibrionaceae* and *Streptococcaceae*, while increasing the levels of
587 *Prevotellaceae* and *Erysipelotrichaceae* (Fig 6D, E).

588 At the genus level, *Peptococcus* were decreased in the CBE group (Fig 6F). In the
589 GPE treated group, we observed a decrease of *Desulfovibrio*, *Clostridium sensu*
590 *stricto* and *Lactococcus*, whereas *Allobaculum* and *Roseburia* were increased (Fig
591 6F).

592

593 **Effects on intestinal barrier**

594 HFD feeding and concomitant changes in the gut microbiota are linked to
595 alterations in the intestinal gut barrier function and in the production of
596 antimicrobial peptides. Here we found that HFD lowered the gene expression of
597 the antimicrobial peptide Reg3 γ all along the intestinal tract (Fig 7A and data not
598 shown for jejunum and ileum) and lowered the expression of intectin, encoding a
599 protein involved in the turnover of intestinal mucosa, in the colon (Fig 7B) and
600 jejunum (data not shown).

601 In the colon, CBE tended to increase levels of intectin (Fig 7B) ($p = 0.008$ versus
602 HFD, Mann-Whitney test), of the antimicrobial peptides Lyz1 ($p = 0.03$) (Fig 7F)
603 and of the tight-junction protein claudin3 ($p = 0.03$) (Fig 7E) compared to the

604 HFD group. Levels of the microbicidal protein Ang4 were higher in the HFD-CBE
605 group as compared to CT mice (Fig 7G). HFD-GPE treatment normalized the
606 levels of Reg3 γ ($p = 0.02$ versus HFD, Mann-Whitney test) (Fig 7A) in the colon
607 and significantly increased the levels of Lyz1 (Fig 7F). The tight junction protein
608 Occludin was somewhat higher in the treated groups when compared to CT and
609 HFD mice, but this did not reach significance (Fig 7D). ZO-1 remained unaffected
610 along the gastro-intestinal tract for all the HFD-treated groups (Fig 7C and data
611 not shown).

612

613 **Effects on bile acids**

614 Primary bile acids (BAs) are synthesized by the liver and may be converted into
615 secondary BAs as a result of biotransformation by the intestinal microbiota (53).
616 They serve many important physiological functions, including glucose and lipid
617 metabolism (54). HFD increased total BAs concentration in cecal content ($p =$
618 0.03 versus CT, Mann-Whitney test) and supplementation with CBE further
619 increased cecal content in BAs compared to the HFD group (Fig 8A), although
620 this did not reach statistical significance. Interestingly, this effect was due solely
621 to an increase in conjugated BAs (Fig 8B), since unconjugated BAs levels did not
622 differ between HFD groups (Fig 8C). At the level of individual BAs, we could not
623 pinpoint one specific BA responsible for this increase; it was rather an
624 accumulation of small changes throughout the BA spectrum that contributed to
625 this overall increase (Fig 8D).

626 In portal vein plasma, total BA concentrations tended to be reduced in untreated
627 HFD mice as compared to CT mice, but were higher in the HFD-CBE and HFD-
628 GPE groups than in the HFD group, reaching levels comparable to that of the CT

629 group (Fig 8E). The percentage of conjugated BA tended to be increased in the
630 HFD-GPE ($p = 0.04$ versus HFD, Mann-Whitney test)(Fig 8F), whereas
631 unconjugated BAs tended to be decreased ($p = 0.04$) (Fig 8G). Similar to the
632 cecum, no specific BA changed in concentration in the plasma (Fig 8H).

633 Bile acids are synthesized via the classical pathway under control of cholesterol
634 7 alpha-hydroxylase (CYP7a1) and cholesterol 8 alpha-hydroxylase (CYP8a1), or
635 via alternate pathways, such as the one under control of cholesterol 27-
636 hydroxylase (CYP27a1) and cholesterol 7 beta-hydroxylase (CYP7b1). To
637 determine whether our extracts could affect bile acid production, we measured
638 the mRNA levels of the main factors controlling these pathways in the liver (Fig 9
639 A-F) and ileum (Fig 9 G-H). We found a clear upregulation of CYP7a1 (Fig 9A)
640 and a modest increase of CYP27a1 (Fig 9D) for the HFD-GPE mice, suggesting an
641 increase in bile acid production in this group.

642 In the liver, bile acids can activate FXR, which has been shown to activate the
643 expression of FGF15 in the intestine (55). FGF15 functions as a metabolic
644 hormone, but also signals through FGFR4 in hepatocytes to inhibit expression of
645 CYP7a1 gene, thereby acting as a negative feedback loop. Interestingly FGF15
646 was upregulated in ileum of the HFD and HFD-GPE groups, but not in the HFD-
647 CBE group (Fig 9H). Suggesting an enlarged bile acid pool in these mice. Why this
648 is not reflected in the bile acid content remains to be determined.

649 Discussion

650 Although polyphenols are not strictly required for vital body functions in
651 humans, there is compelling clinical and epidemiological evidence that they
652 significantly reduce the risk of chronic diseases and promote health (7, 56, 57).
653 However, a significant proportion of the population is not consuming sufficient
654 quantities of dietary polyphenols as a result of inadequate vegetable and fruit
655 intake. Therefore, concentrated polyphenol extracts might be valuable dietary
656 supplements offering an interesting additional strategy for metabolic disorders
657 management (12, 58, 59).

658 In this study, we demonstrated that both cinnamon bark and grape pomace
659 extracts are able to ameliorate the overall metabolic profile in a model of diet-
660 induced obesity. This is evidenced by a decrease in fat mass gain and adipose
661 tissue inflammation and by reduced hepatic lipid content, especially in the grape
662 pomace-treated mice, which was not compensated by elevated plasma lipid
663 concentrations. Our data are consistent with previous reports that showed
664 moderate but significant beneficial effect of table grape extracts on adiposity,
665 hepatic steatosis, insulin resistance and adipose tissue inflammation (28, 30, 60-
666 63).

667 We also found a clear improvement of glucose homeostasis by both extracts, as
668 evidenced by an improved glucose tolerance and lower insulin resistance index.
669 This was associated with a marked reduction of non-esterified fatty acids
670 (NEFAs, free fatty acids), which have previously been found to be modulators of
671 insulin sensitivity (64). Interestingly, although improvement of insulin resistance
672 index was achieved by both grape and cinnamon extracts, the mechanisms

673 behind this seem to be different. Indeed, the HFD-GPE mice needed less insulin
674 to achieve the same overall glucose profile, while the HFD-CBE mice had similar
675 insulin secretion as HFD treated mice, but achieved faster glucose uptake. It has
676 been proposed that cinnamon facilitates glucose entrance into cells by inducing
677 glucose transporter 4 (GLUT4) translocation to the plasma membrane mediated
678 by the LKB1-AMPK signalling pathway (65, 66), whereas grapes might activate
679 the PI3K pathway and promote insulin action by reducing serine kinase
680 activation and cytokine signaling (67). Our data thus suggest that both extracts
681 might be useful additives in the management of glucose homeostasis in diabetic
682 patients, as has been proposed previously (21, 23-25, 27).

683 A large fraction of dietary polyphenols reaches the colon and can be metabolized
684 by the intestinal microbiota. Moreover, polyphenols are well known to affect
685 intestinal bacteria (10, 11). Here, we report a significant impact of our extracts
686 on the microbial composition, which was more profound for the GPE than for the
687 CBE. One of the genera significantly increased by the GPE is *Roseburia*. These are
688 bacteria that were previously found to be at a low abundance in patients with
689 type 2 diabetes and proposed to play an important role in gut health as they have
690 anti-inflammatory effects in the gut (68-70). Interestingly, *Roseburia* are
691 increased by prebiotics and associated with improvements in metabolic
692 disorders (71, 72). We also found a higher abundance of *Allobaculum*
693 (*Erysipelotrichaceae*). This genus has also been shown to be increased by
694 prebiotics (73, 74) and grape extracts (28), and has been associated with
695 improved intestinal integrity, increased Reg3 γ levels in the colon and with
696 resistance to NAFLD development (50). Moreover, Metformin and Berberine,
697 two clinically effective drugs for the treatment of diabetes, are associated with

698 increases in *Allobaculum* abundance (75). As for *Roseburia*, the major end
699 product of *Allobaculum* fermentation is butyrate. This SCFA is of particular
700 relevance in the gut because it is rapidly taken up by enterocytes where it serves
701 as energy source (76). Conflicting data exist about the modulation of SCFA by
702 polyphenols. Some studies reported an increase in SCFA after supplementation
703 of the diet with extracts or phenolic compounds, whereas other studies showed
704 no differences (77), but cecal SCFA content was not affected by treatments in our
705 study (Fig 10A, B, D). GPE contains about 420 mg/g of fibers, which could be
706 insufficient to induce a significant change in the microbial fermentation to
707 markedly affect SCFA production. Alternatively, utilization of short-chain fatty
708 acids by the colonocytes may be more important in this group. This is supported
709 by the drastic increase of SLC5a8, a butyrate transporter, in the colon (Fig 10C).

710 As previously described, HFD feeding increased the abundance of
711 Desulfovibrionaceae (73, 78) and *Lactococcus* (79). This was completely
712 reversed with GPE. Several genera belonging to the Desulfovibrionaceae family
713 are considered opportunistic pathogens and have been linked to some
714 inflammatory diseases (80, 81). They produce endotoxins and have the capacity
715 to reduce sulphate to H₂S (82), thereby damaging the intestinal barrier (83).
716 Indeed, H₂S has been shown to disrupt energy metabolism in the gut epithelium
717 (84). This leads to cell death and ultimately results in intestinal inflammation
718 (85). As for the HFD-CBE mice, we found similar trends for *Roseburia*,
719 *Desulfovibrio* and *Lactococcus* genera as in the HFD-GPE mice, although they did
720 not reach statistical significance. While the genus *Peptococcus* was not
721 consistently increased by HFD, we observed that CBE strongly decreased its
722 level.

723 Previous studies have shown a strong association between the ingestion of
724 polyphenol extracts and the species *Akkermansia muciniphila*, a bacterium
725 known to improve metabolic disorders (12, 58). However, none of the tested
726 treatments were associated with a modulation of *A. muciniphila* (data not
727 shown). This was unexpected, as previous studies have shown an increase in
728 abundance of *A. muciniphila* following polyphenol treatment (reviewed in (58)).
729 In contrast, a recent study using a grape seed extract showed no changes in *A.*
730 *muciniphila* (86) and it was also reported that Resveratrol, a polyphenol mainly
731 found in grapes, berries and a wide range of fruits, decreases *A. muciniphila* in
732 mice (87). In vitro, a pomegranate extract significantly inhibited the growth of *A.*
733 *muciniphila* (88). This may suggest that polyphenols have varied prebiotic
734 potential on *A. muciniphila*. However, there are several design differences
735 between the studies that may have contributed to the divergent results
736 concerning the gut microbiota composition. First, depending on the origin of the
737 polyphenols (for example the grape terroir) and the extraction procedure the
738 composition of the final extracts may vary significantly. Secondly, it has been
739 shown that gut microbiota composition is affected by diet (type and amount of
740 fat/sugar in the diet), mouse strain and age, and mouse provider (89). Thirdly,
741 the increase of a certain bacterial species, such as *A. muciniphila*, may depend on
742 its baseline intestinal abundance.

743 In accordance with our previous findings and the changes in the gut
744 microbiota composition, the expression of several antimicrobial peptides,
745 including Ang4 (effective against Gram-positive and Gram-negative bacteria),
746 Reg3 γ (effective against Gram-positive bacteria), and Lyz1 (mostly effective
747 against Gram-positive bacteria) was found to be increased in response to both

748 CBE and GPE supplementation (90). In the CBE-treated group, this was
749 accompanied by a putative increase in intestinal mucosal turnover and barrier
750 integrity in the colon, as evidenced by an increase of intectin and claudin3.
751 Gut microbiota may affect metabolic parameters by influencing the bile acid pool
752 composition. Bile acids facilitate the digestion and absorption of lipids, but they
753 also act as signaling molecules by binding to FXR, contributing to the regulation
754 of various metabolic processes (91). Bile acid content tended to be increased
755 with CBE, solely due to an increase in conjugated bile acids, suggesting a
756 decrease in bile salt hydrolase (BSH) activity within the microbial community.
757 This seems to be supported by the fact that we did not find any effect on the
758 biological markers associated with the synthesis of bile acids in this group. In
759 addition, evidence has revealed that bile acids are also able to alter the gut
760 microbiota via direct and indirect antimicrobial effects (92), and promote the
761 survival of some bile acid-tolerant bacteria such as
762 some *Lactobacillus* and *Bifidobacterium* species (93). In contrast, we found
763 evidence for an increase bile acid production in GPE treated mice. However, this
764 was not translated to higher bile acid contents in caecum of plasma.
765 Taken together, our data demonstrate that polyphenols derived from grapes or
766 cinnamon can partially counter the deleterious effects of HFD and ameliorate
767 overall metabolic parameters related to adiposity, glucose homeostasis and gut
768 barrier integrity. These changes are associated with a modulation of the
769 microbiota composition and a reduction in inflammation. Interestingly, all these
770 beneficial effects resemble that of prebiotics, even though the doses used were
771 much lower than those generally required for classical prebiotics (59, 94).

772 Modes of action of both compounds were found to be different, indicating that
773 polyphenols have a broad range of targets that require further investigations.
774 Thus, although both studied extracts positively improve glucose and lipid
775 metabolism and reinforce the gut barrier together with changes in the gut
776 microbiota, it is currently unknown how this beneficial effects occur. The health
777 benefits on the host may be mediated by the microbial production of bioactive
778 polyphenol-derived metabolites and/or by the modulation of the gut microbial
779 community itself. Phenolic analysis indicated that the most abundant
780 anthocyanins found in our grape pomace extract were Malvidin-3-O-glucoside,
781 and Peonidin-3-O-glucoside (Table 2). While the antibesity and antidiabetic
782 effects of anthocyanins have been demonstrated previously (29), the
783 mechanisms by which these effects occur are still not clear and conflicting data
784 still remain. Whether the beneficial effects can be attributed to a specific
785 phenolic component or a single bacteria remains to be determined.
786 Importantly, this study is the first reporting a change in animal gut microbes
787 following treatment with a cinnamon extract, as well as a comprehensive
788 phenotyping

789 In conclusion, our data as well as other reports strongly support the
790 interest to use plant extracts rich in polyphenols to improve metabolic disorders
791 associated with obesity and metabolic disorders.

792 Grants and funding

793 PDC is a research associate at FRS-FNRS (Fonds de la Recherche Scientifique),
794 Belgium. HP and AE are research fellows at FRS-FNRS, Belgium. PDC is the
795 recipient of grants from the FNRS, ERC Starting Grant 2013 (European Research
796 Council, Starting grant 336452-ENIGMO), FRFS-WELBIO under grant: WELBIO-
797 CR-2012S-02R and the Funds Baillet-Latour grant for medical research 2015.
798 CD's researcher position is supported by a FIRST Spin-Off grant from the
799 Walloon Region (convention 1410053).

800

801 Acknowledgments

802 We would like to thank A. Barrois, H. Danthinne, T. Pringels, M. Monnoye, C.
803 Philippe and S. Boudebouze for excellent technical assistance. We thank R-M.
804 Goebbels for the processing of the samples prior to histological analysis. We
805 thank E. Bourny from the Laboratoire Provençal des Plantes Aromatiques
806 (LPPAM), Buis les Baronnies, France, for the analysis of cinnamon extract.

807

808 Conflict of interests

809 PileJe (Saint-Laurent-des-Autels, France) provided funding for this study to PDC,
810 PG and EM. AB, AG are employed by PiLeJe. There are no patents or products in
811 development to declare.

- 813 1. <http://www.who.int/mediacentre/factsheets/fs311/en/>.
- 814 2. **Bogardus C.** Missing heritability and GWAS utility. *Obesity (Silver Spring)*
815 17: 209-210, 2009.
- 816 3. **Pi-Sunyer X.** The medical risks of obesity. *Postgrad Med* 121: 21-33,
817 2009.
- 818 4. **Christian JG, Tsai AG, and Bessesen DH.** Interpreting weight losses from
819 lifestyle modification trials: using categorical data. *Int J Obes (Lond)* 34: 207-209,
820 2010.
- 821 5. **Patel D.** Pharmacotherapy for the management of obesity. *Metabolism* 64:
822 1376-1385, 2015.
- 823 6. **Thaiss CA, Itav S, Rothschild D, Meijer M, Levy M, Moresi C,**
824 **Dohnalova L, Braverman S, Rozin S, Malitsky S, Dori-Bachash M, Kuperman**
825 **Y, Biton I, Gertler A, Harmelin A, Shapiro H, Halpern Z, Aharoni A, Segal E,**
826 **and Elinav E.** Persistent microbiome alterations modulate the rate of post-
827 dieting weight regain. *Nature* 2016.
- 828 7. **Del Rio D, Rodriguez-Mateos A, Spencer JP, Tognolini M, Borges G,**
829 **and Crozier A.** Dietary (poly)phenolics in human health: structures,
830 bioavailability, and evidence of protective effects against chronic diseases.
831 *Antioxid Redox Signal* 18: 1818-1892, 2013.
- 832 8. **Chuang CC, and McIntosh MK.** Potential mechanisms by which
833 polyphenol-rich grapes prevent obesity-mediated inflammation and metabolic
834 diseases. *Annu Rev Nutr* 31: 155-176, 2011.
- 835 9. **Selma MV, Espin JC, and Tomas-Barberan FA.** Interaction between
836 phenolics and gut microbiota: role in human health. *J Agric Food Chem* 57: 6485-
837 6501, 2009.
- 838 10. **Nohynek LJ, Alakomi HL, Kahkonen MP, Heinonen M, Helander IM,**
839 **Oksman-Caldentey KM, and Puupponen-Pimia RH.** Berry phenolics:
840 antimicrobial properties and mechanisms of action against severe human
841 pathogens. *Nutr Cancer* 54: 18-32, 2006.
- 842 11. **Puupponen-Pimia R, Nohynek L, Meier C, Kahkonen M, Heinonen M,**
843 **Hopia A, and Oksman-Caldentey KM.** Antimicrobial properties of phenolic
844 compounds from berries. *J Appl Microbiol* 90: 494-507, 2001.
- 845 12. **Anhe FF, Roy D, Pilon G, Dudonne S, Matamoros S, Varin TV, Garofalo**
846 **C, Moine Q, Desjardins Y, Levy E, and Marette A.** A polyphenol-rich cranberry
847 extract protects from diet-induced obesity, insulin resistance and intestinal
848 inflammation in association with increased Akkermansia spp. population in the
849 gut microbiota of mice. *Gut* 64: 872-883, 2015.
- 850 13. **Cani PD, Dewever C, and Delzenne NM.** Inulin-type fructans modulate
851 gastrointestinal peptides involved in appetite regulation (glucagon-like peptide-
852 1 and ghrelin) in rats. *Br J Nutr* 92: 521-526, 2004.
- 853 14. **Backhed F, Ding H, Wang T, Hooper LV, Koh GY, Nagy A, Semenkovich**
854 **CF, and Gordon JL.** The gut microbiota as an environmental factor that regulates
855 fat storage. *Proc Natl Acad Sci U S A* 101: 15718-15723, 2004.
- 856 15. **Turnbaugh PJ, Ley RE, Mahowald MA, Magrini V, Mardis ER, and**
857 **Gordon JL.** An obesity-associated gut microbiome with increased capacity for
858 energy harvest. *Nature* 444: 1027-1031, 2006.

- 859 16. **Rabot S, Membrez M, Bruneau A, Gerard P, Harach T, Moser M,**
860 **Raymond F, Mansourian R, and Chou CJ.** Germ-free C57BL/6J mice are
861 resistant to high-fat-diet-induced insulin resistance and have altered cholesterol
862 metabolism. *FASEB J* 24: 4948-4959, 2010.
- 863 17. **Cani PD, Amar J, Iglesias MA, Poggi M, Knauf C, Bastelica D, Neyrinck**
864 **AM, Fava F, Tuohy KM, Chabo C, Waget A, Delmee E, Cousin B, Sulpice T,**
865 **Chamontin B, Ferrieres J, Tanti JF, Gibson GR, Casteilla L, Delzenne NM,**
866 **Alessi MC, and Burcelin R.** Metabolic endotoxemia initiates obesity and insulin
867 resistance. *Diabetes* 56: 1761-1772, 2007.
- 868 18. **Cani PD, Bibiloni R, Knauf C, Waget A, Neyrinck AM, Delzenne NM,**
869 **and Burcelin R.** Changes in gut microbiota control metabolic endotoxemia-
870 induced inflammation in high-fat diet-induced obesity and diabetes in mice.
871 *Diabetes* 57: 1470-1481, 2008.
- 872 19. **Cani PD.** Metabolism in 2013: The gut microbiota manages host
873 metabolism. *Nat Rev Endocrinol* 10: 74-76, 2014.
- 874 20. **Cani PD, and Everard A.** Talking microbes: When gut bacteria interact
875 with diet and host organs. *Mol Nutr Food Res* 60: 58-66, 2016.
- 876 21. **Liu Y, Cotillard A, Vazier C, Bastard JP, Fellahi S, Stevant M, Allatif O,**
877 **Langlois C, Bieuvelet S, Brochot A, Guilbot A, Clement K, and Rizkalla SW.** A
878 Dietary Supplement Containing Cinnamon, Chromium and Carnosine Decreases
879 Fasting Plasma Glucose and Increases Lean Mass in Overweight or Obese Pre-
880 Diabetic Subjects: A Randomized, Placebo-Controlled Trial. *PLoS One* 10:
881 e0138646, 2015.
- 882 22. **Qin B, Dawson H, Polansky MM, and Anderson RA.** Cinnamon extract
883 attenuates TNF-alpha-induced intestinal lipoprotein ApoB48 overproduction by
884 regulating inflammatory, insulin, and lipoprotein pathways in enterocytes. *Horm*
885 *Metab Res* 41: 516-522, 2009.
- 886 23. **Qin B, Nagasaki M, Ren M, Bajotto G, Oshida Y, and Sato Y.** Cinnamon
887 extract (traditional herb) potentiates in vivo insulin-regulated glucose utilization
888 via enhancing insulin signaling in rats. *Diabetes Res Clin Pract* 62: 139-148, 2003.
- 889 24. **Qin B, Nagasaki M, Ren M, Bajotto G, Oshida Y, and Sato Y.** Cinnamon
890 extract prevents the insulin resistance induced by a high-fructose diet. *Horm*
891 *Metab Res* 36: 119-125, 2004.
- 892 25. **Ziegenfuss TN, Hofheins JE, Mendel RW, Landis J, and Anderson RA.**
893 Effects of a water-soluble cinnamon extract on body composition and features of
894 the metabolic syndrome in pre-diabetic men and women. *J Int Soc Sports Nutr* 3:
895 45-53, 2006.
- 896 26. **Ranasinghe P, Jayawardana R, Galappaththy P, Constantine GR, de**
897 **Vas Gunawardana N, and Katulanda P.** Efficacy and safety of 'true' cinnamon
898 (*Cinnamomum zeylanicum*) as a pharmaceutical agent in diabetes: a systematic
899 review and meta-analysis. *Diabet Med* 29: 1480-1492, 2012.
- 900 27. **Akaberi M, and Hosseinzadeh H.** Grapes (*Vitis vinifera*) as a Potential
901 Candidate for the Therapy of the Metabolic Syndrome. *Phytother Res* 30: 540-
902 556, 2016.
- 903 28. **Collins B, Hoffman J, Martinez K, Grace M, Lila MA, Cockrell C,**
904 **Nadimpalli A, Chang E, Chuang CC, Zhong W, Mackert J, Shen W, Cooney P,**
905 **Hopkins R, and McIntosh M.** A polyphenol-rich fraction obtained from table
906 grapes decreases adiposity, insulin resistance and markers of inflammation and
907 impacts gut microbiota in high-fat-fed mice. *J Nutr Biochem* 31: 150-165, 2016.

- 908 29. **He J, and Giusti MM.** Anthocyanins: natural colorants with health-
 909 promoting properties. *Annu Rev Food Sci Technol* 1: 163-187, 2010.
- 910 30. **Baldwin J, Collins B, Wolf PG, Martinez K, Shen W, Chuang CC, Zhong**
 911 **W, Cooney P, Cockrell C, Chang E, Gaskins HR, and McIntosh MK.** Table grape
 912 consumption reduces adiposity and markers of hepatic lipogenesis and alters gut
 913 microbiota in butter fat-fed mice. *J Nutr Biochem* 27: 123-135, 2016.
- 914 31. **Roopchand DE, Carmody RN, Kuhn P, Moskal K, Rojas-Silva P,**
 915 **Turnbaugh PJ, and Raskin I.** Dietary Polyphenols Promote Growth of the Gut
 916 Bacterium *Akkermansia muciniphila* and Attenuate High-Fat Diet-Induced
 917 Metabolic Syndrome. *Diabetes* 64: 2847-2858, 2015.
- 918 32. **Wang H, Xue Y, Zhang H, Huang Y, Yang G, Du M, and Zhu MJ.** Dietary
 919 grape seed extract ameliorates symptoms of inflammatory bowel disease in
 920 IL10-deficient mice. *Mol Nutr Food Res* 57: 2253-2257, 2013.
- 921 33. **Anderson RA, Broadhurst CL, Polansky MM, Schmidt WF, Khan A,**
 922 **Flanagan VP, Schoene NW, and Graves DJ.** Isolation and characterization of
 923 polyphenol type-A polymers from cinnamon with insulin-like biological activity. *J*
 924 *Agric Food Chem* 52: 65-70, 2004.
- 925 34. **Kammerer D, Claus A, Carle R, and Schieber A.** Polyphenol screening of
 926 pomace from red and white grape varieties (*Vitis vinifera* L.) by HPLC-DAD-
 927 MS/MS. *J Agric Food Chem* 52: 4360-4367, 2004.
- 928 35. **Cani PD, Amar J, Iglesias MA, Poggi M, Knauf C, Bastelica D, Neyrinck**
 929 **AM, Fava F, Tuohy KM, Chabo C, Waget A, Delmee E, Cousin B, Sulpice T,**
 930 **Chamontin B, Ferrieres J, Tanti JF, Gibson GR, Casteilla L, Delzenne NM,**
 931 **Alessi MC, and Burcelin R.** Metabolic endotoxemia initiates obesity and insulin
 932 resistance. *Diabetes* 56: 1761-1772, 2007.
- 933 36. **Geurts L, Everard A, Van Hul M, Essaghir A, Duparc T, Matamoros S,**
 934 **Plovier H, Castel J, Denis RG, Bergiers M, Druart C, Alhouayek M, Delzenne**
 935 **NM, Muccioli GG, Demoulin JB, Luquet S, and Cani PD.** Adipose tissue NAPE-
 936 PLD controls fat mass development by altering the browning process and gut
 937 microbiota. *Nat Commun* 6: 6495, 2015.
- 938 37. **Everard A, Geurts L, Caesar R, Van Hul M, Matamoros S, Duparc T,**
 939 **Denis RG, Cochez P, Pierard F, Castel J, Bindels LB, Plovier H, Robine S,**
 940 **Muccioli GG, Renauld JC, Dumoutier L, Delzenne NM, Luquet S, Backhed F,**
 941 **and Cani PD.** Intestinal epithelial MyD88 is a sensor switching host metabolism
 942 towards obesity according to nutritional status. *Nat Commun* 5: 5648, 2014.
- 943 38. **Folch J, Lees M, and Sloane Stanley GH.** A simple method for the
 944 isolation and purification of total lipides from animal tissues. *J Biol Chem* 226:
 945 497-509, 1957.
- 946 39. **Lan A, Bruneau A, Bensaada M, Philippe C, Bellaud P, Rabot S, and Jan**
 947 **G.** Increased induction of apoptosis by *Propionibacterium freudenreichii* TL133
 948 in colonic mucosal crypts of human microbiota-associated rats treated with 1,2-
 949 dimethylhydrazine. *Br J Nutr* 100: 1251-1259, 2008.
- 950 40. **Tremaroli V, Karlsson F, Werling M, Stahlman M, Kovatcheva-**
 951 **Datchary P, Olbers T, Fandriks L, le Roux CW, Nielsen J, and Backhed F.**
 952 Roux-en-Y Gastric Bypass and Vertical Banded Gastroplasty Induce Long-Term
 953 Changes on the Human Gut Microbiome Contributing to Fat Mass Regulation. *Cell*
 954 *Metab* 22: 228-238, 2015.
- 955 41. **Magoc T, and Salzberg SL.** FLASH: fast length adjustment of short reads
 956 to improve genome assemblies. *Bioinformatics* 27: 2957-2963, 2011.

- 957 42. **Schloss PD, Westcott SL, Ryabin T, Hall JR, Hartmann M, Hollister EB,**
958 **Lesniewski RA, Oakley BB, Parks DH, Robinson CJ, Sahl JW, Stres B,**
959 **Thallinger GG, Van Horn DJ, and Weber CF.** Introducing mothur: open-source,
960 platform-independent, community-supported software for describing and
961 comparing microbial communities. *Appl Environ Microbiol* 75: 7537-7541, 2009.
- 962 43. **Edgar RC, Haas BJ, Clemente JC, Quince C, and Knight R.** UCHIME
963 improves sensitivity and speed of chimera detection. *Bioinformatics* 27: 2194-
964 2200, 2011.
- 965 44. **Sun Y, Cai Y, Huse SM, Knight R, Farmerie WG, Wang X, and Mai V.** A
966 large-scale benchmark study of existing algorithms for taxonomy-independent
967 microbial community analysis. *Brief Bioinform* 13: 107-121, 2011.
- 968 45. **DeSantis TZ, Hugenholtz P, Larsen N, Rojas M, Brodie EL, Keller K,**
969 **Huber T, Dalevi D, Hu P, and Andersen GL.** Greengenes, a chimera-checked
970 16S rRNA gene database and workbench compatible with ARB. *Appl Environ*
971 *Microbiol* 72: 5069-5072, 2006.
- 972 46. **Wang Q, Garrity GM, Tiedje JM, and Cole JR.** Naive Bayesian classifier
973 for rapid assignment of rRNA sequences into the new bacterial taxonomy. *Appl*
974 *Environ Microbiol* 73: 5261-5267, 2007.
- 975 47. **Hochberg Y, and Benjamini Y.** More powerful procedures for multiple
976 significance testing. *Stat Med* 9: 811-818, 1990.
- 977 48. **Kanda H, Tateya S, Tamori Y, Kotani K, Hiasa K, Kitazawa R, Kitazawa**
978 **S, Miyachi H, Maeda S, Egashira K, and Kasuga M.** MCP-1 contributes to
979 macrophage infiltration into adipose tissue, insulin resistance, and hepatic
980 steatosis in obesity. *J Clin Invest* 116: 1494-1505, 2006.
- 981 49. **Patsouris D, Li PP, Thapar D, Chapman J, Olefsky JM, and Neels JG.**
982 Ablation of CD11c-positive cells normalizes insulin sensitivity in obese insulin
983 resistant animals. *Cell Metab* 8: 301-309, 2008.
- 984 50. **Le Roy T, Llopis M, Lepage P, Bruneau A, Rabot S, Bevilacqua C,**
985 **Martin P, Philippe C, Walker F, Bado A, Perlemuter G, Cassard-Doulier AM,**
986 **and Gerard P.** Intestinal microbiota determines development of non-alcoholic
987 fatty liver disease in mice. *Gut* 62: 1787-1794, 2013.
- 988 51. **Backhed F, Manchester JK, Semenkovich CF, and Gordon JI.**
989 Mechanisms underlying the resistance to diet-induced obesity in germ-free mice.
990 *Proc Natl Acad Sci U S A* 104: 979-984, 2007.
- 991 52. **Cani PD, Possemiers S, Van de Wiele T, Guiot Y, Everard A, Rottier O,**
992 **Geurts L, Naslain D, Neyrinck A, Lambert DM, Muccioli GG, and Delzenne**
993 **NM.** Changes in gut microbiota control inflammation in obese mice through a
994 mechanism involving GLP-2-driven improvement of gut permeability. *Gut* 58:
995 1091-1103, 2009.
- 996 53. **Gerard P.** Metabolism of cholesterol and bile acids by the gut microbiota.
997 *Pathogens* 3: 14-24, 2013.
- 998 54. **Sayin SI, Wahlstrom A, Felin J, Jantti S, Marschall HU, Bamberg K,**
999 **Angelin B, Hyotylainen T, Oresic M, and Backhed F.** Gut microbiota regulates
1000 bile acid metabolism by reducing the levels of tauro-beta-muricholic acid, a
1001 naturally occurring FXR antagonist. *Cell Metab* 17: 225-235, 2013.
- 1002 55. **Inagaki T, Choi M, Moschetta A, Peng L, Cummins CL, McDonald JG,**
1003 **Luo G, Jones SA, Goodwin B, Richardson JA, Gerard RD, Repa JJ, Mangelsdorf**
1004 **DJ, and Kliewer SA.** Fibroblast growth factor 15 functions as an enterohepatic
1005 signal to regulate bile acid homeostasis. *Cell Metab* 2: 217-225, 2005.

- 1006 56. **Blade C, Aragonés G, Arola-Arnal A, Muguerza B, Bravo FI, Salvado**
1007 **MJ, Arola L, and Suarez M.** Proanthocyanidins in health and disease. *Biofactors*
1008 42: 5-12, 2016.
- 1009 57. **Zhang PY.** Polyphenols in Health and Disease. *Cell Biochem Biophys* 73:
1010 649-664, 2015.
- 1011 58. **Anhe FF, Pilon G, Roy D, Desjardins Y, Levy E, and Marette A.**
1012 Triggering Akkermansia with dietary polyphenols: A new weapon to combat the
1013 metabolic syndrome? *Gut Microbes* 7: 146-153, 2016.
- 1014 59. **Anhe FF, Varin TV, Le Barz M, Desjardins Y, Levy E, Roy D, and**
1015 **Marette A.** Gut Microbiota Dysbiosis in Obesity-Linked Metabolic Diseases and
1016 Prebiotic Potential of Polyphenol-Rich Extracts. *Curr Obes Rep* 4: 389-400, 2015.
- 1017 60. **Suwannaphet W, Meeprom A, Yibchok-Anun S, and Adisakwattana S.**
1018 Preventive effect of grape seed extract against high-fructose diet-induced insulin
1019 resistance and oxidative stress in rats. *Food Chem Toxicol* 48: 1853-1857, 2010.
- 1020 61. **Park SH, Park TS, and Cha YS.** Grape seed extract (*Vitis vinifera*)
1021 partially reverses high fat diet-induced obesity in C57BL/6J mice. *Nutr Res Pract*
1022 2: 227-233, 2008.
- 1023 62. **Terra X, Pallares V, Ardevol A, Blade C, Fernandez-Larrea J, Pujadas**
1024 **G, Salvado J, Arola L, and Blay M.** Modulatory effect of grape-seed procyanidins
1025 on local and systemic inflammation in diet-induced obesity rats. *J Nutr Biochem*
1026 22: 380-387, 2011.
- 1027 63. **Gourineni V, Shay NF, Chung S, Sandhu AK, and Gu L.** Muscadine grape
1028 (*Vitis rotundifolia*) and wine phytochemicals prevented obesity-associated
1029 metabolic complications in C57BL/6J mice. *J Agric Food Chem* 60: 7674-7681,
1030 2012.
- 1031 64. **Kahn SE, Hull RL, and Utzschneider KM.** Mechanisms linking obesity to
1032 insulin resistance and type 2 diabetes. *Nature* 444: 840-846, 2006.
- 1033 65. **Absalan A, Mohiti-Ardakani J, Hadinedoushan H, and Khalili MA.**
1034 Hydro-Alcoholic Cinnamon Extract, Enhances Glucose Transporter Isotype-4
1035 Translocation from Intracellular Compartments into the Cytoplasmic Membrane
1036 of C2C12 Myotubes. *Indian J Clin Biochem* 27: 351-356, 2012.
- 1037 66. **Shen Y, Honma N, Kobayashi K, Jia LN, Hosono T, Shindo K, Ariga T,**
1038 **and Seki T.** Cinnamon extract enhances glucose uptake in 3T3-L1 adipocytes
1039 and C2C12 myocytes by inducing LKB1-AMP-activated protein kinase signaling.
1040 *PLoS One* 9: e87894, 2014.
- 1041 67. **Yogalakshmi B, Bhuvaneshwari S, Sreeja S, and Anuradha CV.** Grape
1042 seed proanthocyanidins and metformin act by different mechanisms to promote
1043 insulin signaling in rats fed high calorie diet. *J Cell Commun Signal* 8: 13-22, 2014.
- 1044 68. **Aminov RI, Walker AW, Duncan SH, Harmsen HJ, Welling GW, and**
1045 **Flint HJ.** Molecular diversity, cultivation, and improved detection by fluorescent
1046 in situ hybridization of a dominant group of human gut bacteria related to
1047 *Roseburia* spp. or *Eubacterium rectale*. *Appl Environ Microbiol* 72: 6371-6376,
1048 2006.
- 1049 69. **Karlsson FH, Tremaroli V, Nookaew I, Bergstrom G, Behre CJ,**
1050 **Fagerberg B, Nielsen J, and Backhed F.** Gut metagenome in European women
1051 with normal, impaired and diabetic glucose control. *Nature* 498: 99-103, 2013.
- 1052 70. **Qin J, Li Y, Cai Z, Li S, Zhu J, Zhang F, Liang S, Zhang W, Guan Y, Shen D,**
1053 **Peng Y, Zhang D, Jie Z, Wu W, Qin Y, Xue W, Li J, Han L, Lu D, Wu P, Dai Y, Sun**
1054 **X, Li Z, Tang A, Zhong S, Li X, Chen W, Xu R, Wang M, Feng Q, Gong M, Yu J,**

- 1055 **Zhang Y, Zhang M, Hansen T, Sanchez G, Raes J, Falony G, Okuda S, Almeida**
 1056 **M, LeChatelier E, Renault P, Pons N, Batto JM, Zhang Z, Chen H, Yang R,**
 1057 **Zheng W, Li S, Yang H, Wang J, Ehrlich SD, Nielsen R, Pedersen O,**
 1058 **Kristiansen K, and Wang J.** A metagenome-wide association study of gut
 1059 microbiota in type 2 diabetes. *Nature* 490: 55-60, 2012.
- 1060 71. **Neyrinck AM, Possemiers S, Druart C, Van de Wiele T, De Backer F,**
 1061 **Cani PD, Larondelle Y, and Delzenne NM.** Prebiotic effects of wheat
 1062 arabinoxylan related to the increase in bifidobacteria, Roseburia and
 1063 Bacteroides/Prevotella in diet-induced obese mice. *PLoS One* 6: e20944, 2011.
- 1064 72. **Neyrinck AM, Possemiers S, Verstraete W, De Backer F, Cani PD, and**
 1065 **Delzenne NM.** Dietary modulation of clostridial cluster XIVa gut bacteria
 1066 (Roseburia spp.) by chitin-glucan fiber improves host metabolic alterations
 1067 induced by high-fat diet in mice. *J Nutr Biochem* 23: 51-59, 2012.
- 1068 73. **Everard A, Lazarevic V, Gaia N, Johansson M, Stahlman M, Backhed F,**
 1069 **Delzenne NM, Schrenzel J, Francois P, and Cani PD.** Microbiome of prebiotic-
 1070 treated mice reveals novel targets involved in host response during obesity.
 1071 *ISME J* 8: 2116-2130, 2014.
- 1072 74. **Tachon S, Zhou J, Keenan M, Martin R, and Marco ML.** The intestinal
 1073 microbiota in aged mice is modulated by dietary resistant starch and correlated
 1074 with improvements in host responses. *FEMS Microbiol Ecol* 83: 299-309, 2013.
- 1075 75. **Zhang X, Zhao Y, Xu J, Xue Z, Zhang M, Pang X, Zhang X, and Zhao L.**
 1076 Modulation of gut microbiota by berberine and metformin during the treatment
 1077 of high-fat diet-induced obesity in rats. *Sci Rep* 5: 14405, 2015.
- 1078 76. **Donohoe DR, Garge N, Zhang X, Sun W, O'Connell TM, Bunker MK,**
 1079 **and Bultman SJ.** The microbiome and butyrate regulate energy metabolism and
 1080 autophagy in the mammalian colon. *Cell Metab* 13: 517-526, 2011.
- 1081 77. **Mosele JI, Macia A, and Motilva MJ.** Metabolic and Microbial Modulation
 1082 of the Large Intestine Ecosystem by Non-Absorbed Diet Phenolic Compounds: A
 1083 Review. *Molecules* 20: 17429-17468, 2015.
- 1084 78. **Zhang C, Zhang M, Pang X, Zhao Y, Wang L, and Zhao L.** Structural
 1085 resilience of the gut microbiota in adult mice under high-fat dietary
 1086 perturbations. *ISME J* 6: 1848-1857, 2012.
- 1087 79. **Parks BW, Nam E, Org E, Kostem E, Norheim F, Hui ST, Pan C, Civelek**
 1088 **M, Rau CD, Bennett BJ, Mehrabian M, Ursell LK, He A, Castellani LW, Zinker**
 1089 **B, Kirby M, Drake TA, Drevon CA, Knight R, Gargalovic P, Kirchgessner T,**
 1090 **Eskin E, and Lusis AJ.** Genetic control of obesity and gut microbiota composition
 1091 in response to high-fat, high-sucrose diet in mice. *Cell Metab* 17: 141-152, 2013.
- 1092 80. **Loubinoux J, Mory F, Pereira IA, and Le Faou AE.** Bacteremia caused by
 1093 a strain of *Desulfovibrio* related to the provisionally named *Desulfovibrio*
 1094 *fairfieldensis*. *J Clin Microbiol* 38: 931-934, 2000.
- 1095 81. **Weglarz L, Dzierzewicz Z, Skop B, Orchel A, Parfiniewicz B,**
 1096 **Wisniowska B, Swiatkowska L, and Wilczok T.** *Desulfovibrio desulfuricans*
 1097 lipopolysaccharides induce endothelial cell IL-6 and IL-8 secretion and E-selectin
 1098 and VCAM-1 expression. *Cell Mol Biol Lett* 8: 991-1003, 2003.
- 1099 82. **Wagner M, Roger AJ, Flax JL, Brusseau GA, and Stahl DA.** Phylogeny of
 1100 dissimilatory sulfite reductases supports an early origin of sulfate respiration. *J*
 1101 *Bacteriol* 180: 2975-2982, 1998.
- 1102 83. **Jakobsson HE, Rodriguez-Pineiro AM, Schutte A, Ermund A, Boysen P,**
 1103 **Bemark M, Sommer F, Backhed F, Hansson GC, and Johansson ME.** The

- 1104 composition of the gut microbiota shapes the colon mucus barrier. *EMBO Rep* 16:
1105 164-177, 2015.
- 1106 84. **Babidge W, Millard S, and Roediger W.** Sulfides impair short chain fatty
1107 acid beta-oxidation at acyl-CoA dehydrogenase level in colonocytes: implications
1108 for ulcerative colitis. *Mol Cell Biochem* 181: 117-124, 1998.
- 1109 85. **Den Hond E, Hiele M, Evenepoel P, Peeters M, Ghos Y, and Rutgeerts**
1110 **P.** In vivo butyrate metabolism and colonic permeability in extensive ulcerative
1111 colitis. *Gastroenterology* 115: 584-590, 1998.
- 1112 86. **Liu W, Zhao S, Wang J, Shi J, Sun Y, Wang W, Ning G, Hong J, and Liu R.**
1113 Grape seed proanthocyanidin extract ameliorates inflammation and adiposity by
1114 modulating gut microbiota in high-fat diet mice. *Mol Nutr Food Res* 2017.
- 1115 87. **Sung MM, Kim TT, Denou E, Soltys CM, Hamza SM, Byrne NJ, Masson**
1116 **G, Park H, Wishart DS, Madsen KL, Schertzer JD, and Dyck JR.** Improved
1117 Glucose Homeostasis in Obese Mice Treated With Resveratrol Is Associated With
1118 Alterations in the Gut Microbiome. *Diabetes* 66: 418-425, 2017.
- 1119 88. **Henning SM, Summanen PH, Lee RP, Yang J, Finegold SM, Heber D,**
1120 **and Li Z.** Pomegranate ellagitannins stimulate the growth of *Akkermansia*
1121 *muciniphila* in vivo. *Anaerobe* 43: 56-60, 2017.
- 1122 89. **Laukens D, Brinkman BM, Raes J, De Vos M, and Vandenabeele P.**
1123 Heterogeneity of the gut microbiome in mice: guidelines for optimizing
1124 experimental design. *FEMS Microbiol Rev* 40: 117-132, 2016.
- 1125 90. **Gallo RL, and Hooper LV.** Epithelial antimicrobial defence of the skin and
1126 intestine. *Nat Rev Immunol* 12: 503-516, 2012.
- 1127 91. **Wang YD, Chen WD, Moore DD, and Huang W.** FXR: a metabolic
1128 regulator and cell protector. *Cell Res* 18: 1087-1095, 2008.
- 1129 92. **Begley M, Gahan CG, and Hill C.** The interaction between bacteria and
1130 bile. *FEMS Microbiol Rev* 29: 625-651, 2005.
- 1131 93. **Devkota S, Wang Y, Musch MW, Leone V, Fehlner-Peach H,**
1132 **Nadimpalli A, Antonopoulos DA, Jabri B, and Chang EB.** Dietary-fat-induced
1133 taurocholic acid promotes pathobiont expansion and colitis in *Il10*^{-/-} mice.
1134 *Nature* 487: 104-108, 2012.
- 1135 94. **Bindels LB, Delzenne NM, Cani PD, and Walter J.** Towards a more
1136 comprehensive concept for prebiotics. *Nat Rev Gastroenterol Hepatol* 12: 303-
1137 310, 2015.
- 1138
- 1139

1140 Figure Legends

1141

1142 **Figure 1. Effects on body composition and adipose tissue.**

1143 8 week follow up of (A) body weight (g) with corresponding (B) fat mass (g) and
1144 (C) lean mass (g) measured by TD-NMR. (D) Body weight gain (g), (E) fat mass
1145 (g), (F) fat mass and lean mass (% of total body weight) at the end of the follow
1146 up. (G) Weight of brown adipose tissue (mg). (H) Weights of subcutaneous,
1147 epididymal and visceral adipose tissues (mg) and corresponding (I) adiposity
1148 index (%white adipose tissue/body weight). (J) Leptin plasma levels (ng/ml).
1149 Data are presented as the mean±s.e.m. ‘*’ ‘**’ and ‘#’ indicate a significant
1150 difference versus HFD (P<0.05, P<0.01, P<0.001 respectively) as determined by a
1151 two-way ANOVA (A-C). Data with different superscript letters are significantly
1152 different (P<0.05) according to post-hoc one-way ANOVA (D-J).

1153

1154 **Figure 2. Effects on Glucose homeostasis.**

1155 (A) Plasma glucose (mg/dl) profile and (B) the mean area under the curve (AUC)
1156 measured between 0 and 120 min after glucose loading (mg/dl/min). (C) Plasma
1157 insulin levels at 30 min before and 15 min after glucose loading (µg/l). (D)
1158 Glucose-induced insulin secretion, calculated as the difference between the
1159 fasting insulinemia and the insulinemia 15 min after an oral glucose load. (E)
1160 Insulin resistance index determined by multiplying the AUC of blood glucose by
1161 the AUC of insulin between 30 min before and 15 min after glucose loading. (F)
1162 Adipocyte distribution and frequency with respect to the mean diameter
1163 measured by histological analysis. (G) Mean adipocyte size (µm). (H) Resistin
1164 plasma levels measured in the vena cava (ng/ml). Data are presented as the
1165 mean±s.e.m. ‘*’ ‘**’ and ‘#’ indicate a significant difference versus HFD (P<0.05,
1166 P<0.01, P<0.001 respectively) as determined by a two-way ANOVA (A-B). Data
1167 with different superscript letters are significantly different (P<0.05) according to
1168 post-hoc one-way ANOVA (B-E).

1169

1170 **Figure 3. Effects on energy metabolism.**

1171 Energy intake: (A) mean food intake per week per mouse (kcal). Energy
1172 excretion: (B) mean amount of feces excreted per mouse in 24h (mg/24h), (C)
1173 mean energy content in feces (kcal/g) and (D) daily energy excretion as
1174 calculated using the previous values (kcal/mouse) and (E) as percentage of the
1175 food intake. (F) Energy expenditure per night per mouse (kcal/h/kg). (G) Daily
1176 energy expenditure (kCal/h/kg), (H) body temperature (°C) and (I) respiratory
1177 exchange ratio (RER). (J) Cumulative mean number of beam breaks recorded per
1178 mouse during six days. (J) qPCR analysis of glucose transporters SGLT1 and
1179 GLUT2, and of fatty acid transporters LFABP and CD36. Data are presented as the
1180 mean±s.e.m. Data with different superscript letters are significantly different
1181 (P<0.05) according to post-hoc one-way ANOVA (A-E). ‘*’ and ‘**’ indicate a

1182 significant difference versus HFD ($P<0.05$ and $P<0.01$ respectively) as
1183 determined by a two-way ANOVA (F).

1184

1185 **Figure 4. Effects on lipid homeostasis.**

1186 (A) Plasmatic concentrations of non-esterified fatty acids (NEFAs) (mM),
1187 cholesterol (mg/dl) and triglycerides (mg/dl). (B) Hepatic total lipid content
1188 (mg/100mg tissue), cholesterol (mmol/mg tissue) and triglycerides (mmol/mg
1189 tissue),

1190 (C) Representative Oil Red O pictures of the liver with quantitative measurement
1191 (%). Data are presented as the mean \pm s.e.m. Data with different superscript
1192 letters are significantly different ($P<0.05$) according to post-hoc one-way
1193 ANOVA.

1194

1195 **Figure 5. Effects on adipose tissue inflammation.**

1196 qPCR analysis of macrophage markers mRNA expression (A) in the subcutaneous
1197 and (B) the visceral adipose tissue (fold change versus CT group). (C)
1198 Representative staining of MAC2 with Hematoxylin counterstaining of
1199 subcutaneous adipose tissues and quantitative measurements of the mean
1200 number of positive cells per adipocyte counted. (D) Plasma concentrations of
1201 different inflammatory markers. Data are presented as the mean \pm s.e.m. Data
1202 with different superscript letters are significantly different ($P<0.05$) according to
1203 post-hoc one-way ANOVA.

1204

1205 **Figure 6. Effects on gut microbiota.**

1206 Gut bacterial community analysis by 16S rRNA gene high-throughput
1207 sequencing. (A) Composition of abundant bacterial phyla identified in the
1208 microbiota of the four different groups. (B) OTUs significantly affected by grape
1209 or cinnamon supplementation under HFD. A representative 16S rRNA gene from
1210 each of the differentially expressed OTUs versus HFD mice was aligned and used
1211 to infer the phylogenetic trees shown in this figure. The color of the OTU
1212 indicates its family. (C) Principal coordinate analysis based on the weighted
1213 UniFrac analysis (PCoA + WUF) on operational taxonomic units (OTUs). Each
1214 symbol representing a single sample is colored according to the group. (D-E)
1215 Relative abundances (percentage of 16S rRNA gene sequences) of the different
1216 bacterial families in each sample among the CT, HFD, HFD-CBE, HFD-GPE groups.
1217 (F) Relative abundances (percentage of 16S rRNA sequences) of the various
1218 bacterial genera in each sample among each group of mice. Data are presented as
1219 box-plots. . '*' and '**' indicate a significant difference versus HFD ($P<0.05$ and
1220 $P<0.01$ respectively) as determined by the unpaired two-tailed Student's t-test.

1221

1222 **Figure 7. Effects on intestinal barrier.**

1223 (A-J) qPCR analysis of various markers of the intestinal barrier integrity and
1224 anti-microbial peptides in the colon (fold change versus CT group). Data are

1225 expressed as mean±s.e.m. Data with different superscript letters are significantly
1226 different (P<0.05) according to post-hoc one-way ANOVA.

1227

1228

1229 **Figure 8. Effects on bile acids.**

1230 (A) Cecal bile acid concentration (pM/mg cecal content) and percentages of (B)
1231 conjugated and (C) unconjugated bile acids. (D) Cecal bile acids content (% of
1232 total bile acids). (E) Plasma bile acid concentrations (nM) and percentages of (F)
1233 conjugated and (G) unconjugated bile acids. (H) Plasma bile acids content (% of
1234 total bile acids). (CA: cholic acid; LCA: lithocholic acid; UDCA: ursodeoxycholic
1235 acid; CDCA: chenodeoxycholic acid; DCA: deoxycholic acid; MCA: muricholic acid;
1236 T: taurine-; o: omega; a: alpha; b: beta conjugated species). Data are expressed as
1237 mean±s.e.m. Data with different superscript letters are significantly different
1238 (P<0.05) according to post-hoc one-way ANOVA.

1239

1240 **Figure 9. Bile acid production**

1241 qPCR analysis of bile acid production/signaling markers: (A) Cyp7a1, (B)
1242 Cyp7b1, (C) Cyp8a1, (D) cyp27a1, (E) FXR, (F) FGFR4 in the liver. (G) FXR and
1243 (H) FGF15 in the ileum. Data are expressed as mean±s.e.m. Data with different
1244 superscript letters are significantly different (P<0.05) according to post-hoc one-
1245 way ANOVA.

1246

1247 **Figure 10. Cecal short-chain fatty acids (SCFA)**

1248 Concentration of (A) Total short-chain fatty acids (SCFA) content and (B) iso-
1249 SCFA in the caecum (µmol/g cecal content). (C) mRNA levels of the butyrate
1250 transporter SLC5a8 in the colon. (D) Relative concentrations of Acetate, Butyrate
1251 and Propionate (% of total SCFA). Data are expressed as mean±s.e.m. Data with
1252 different superscript letters are significantly different (P<0.05) according to
1253 post-hoc one-way ANOVA.

1254

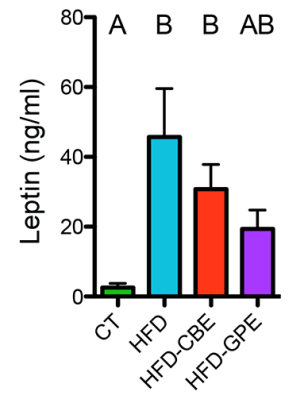
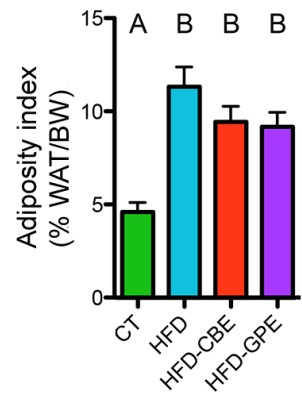
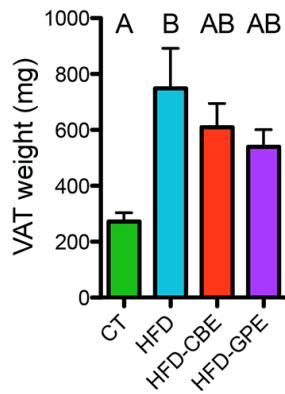
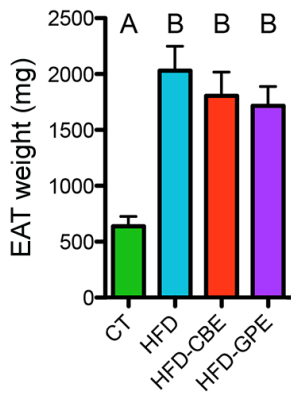
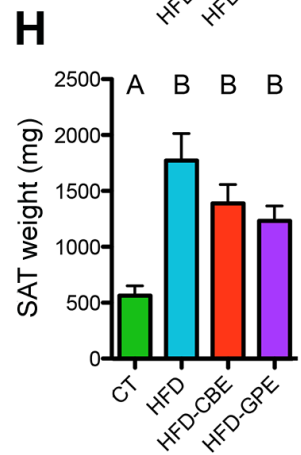
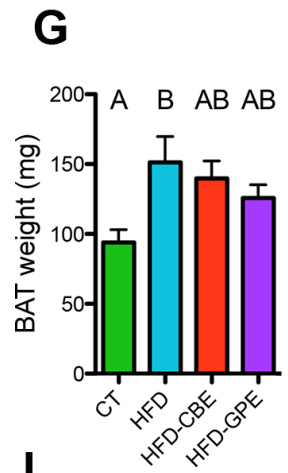
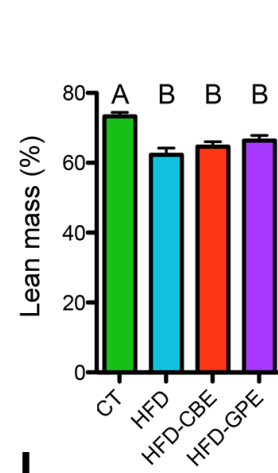
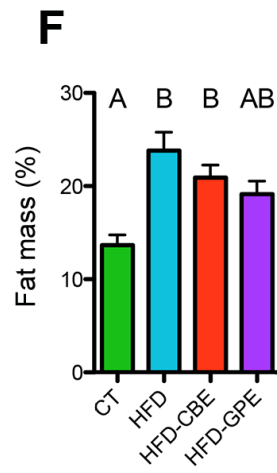
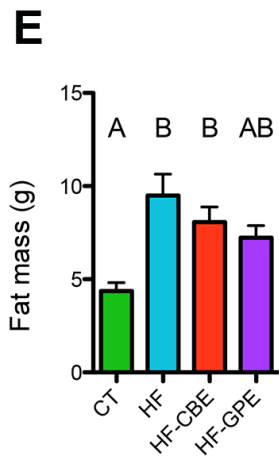
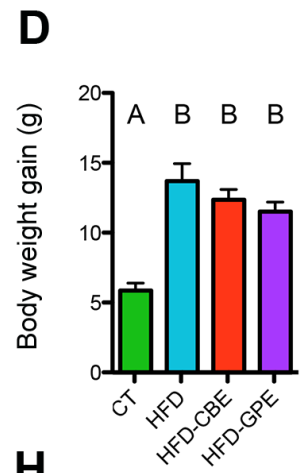
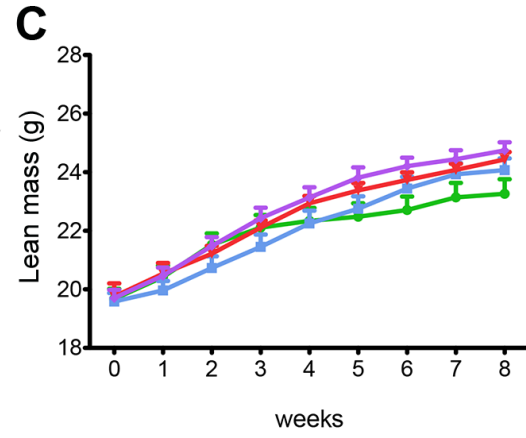
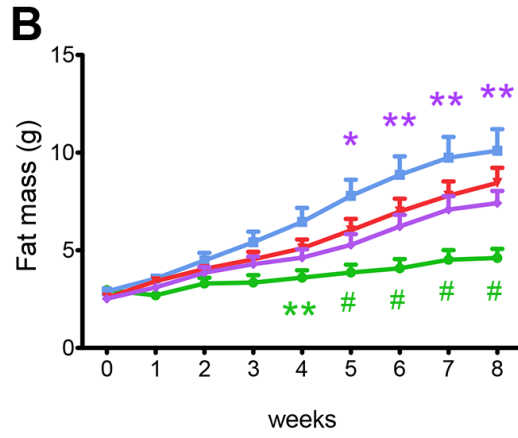
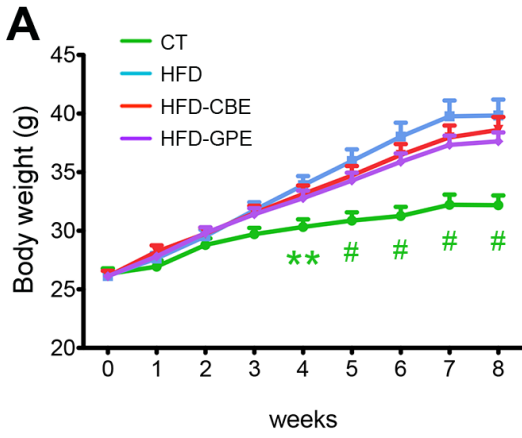
1255 **Table 1**

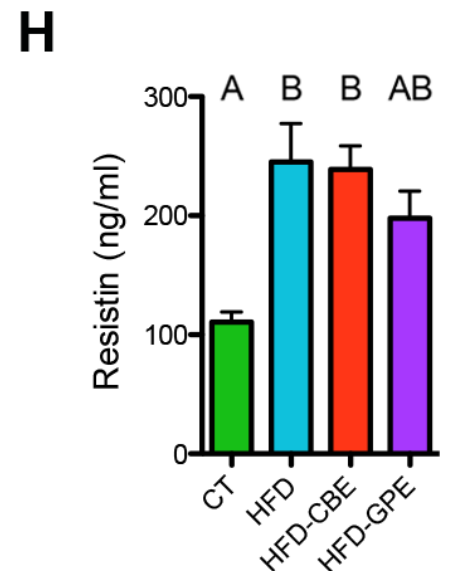
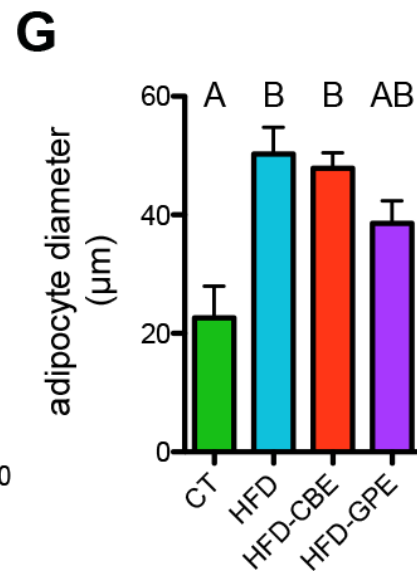
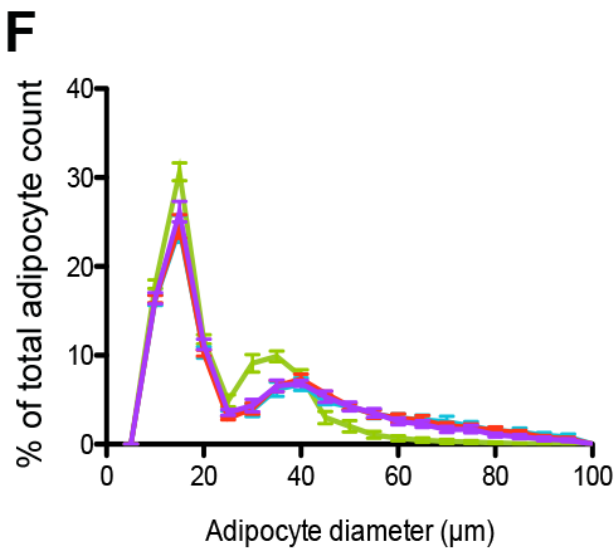
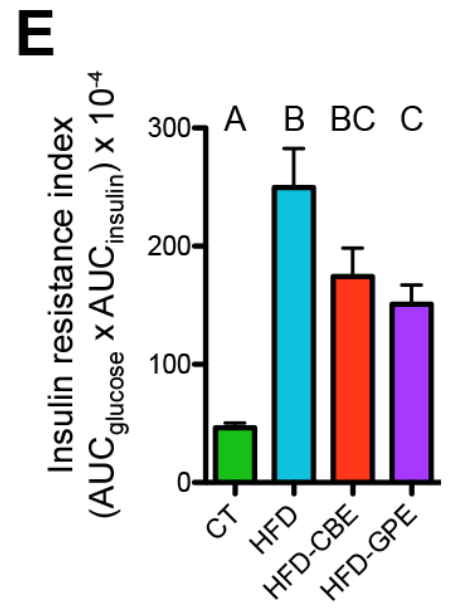
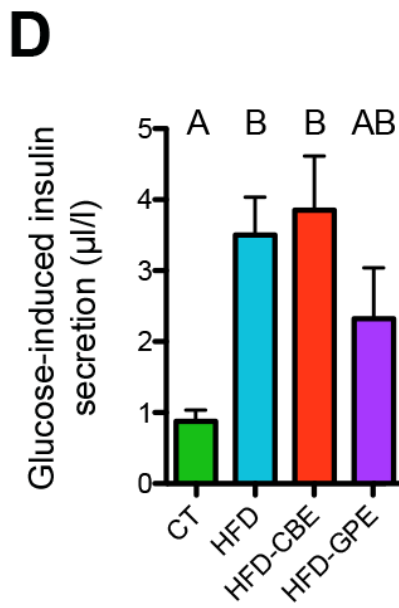
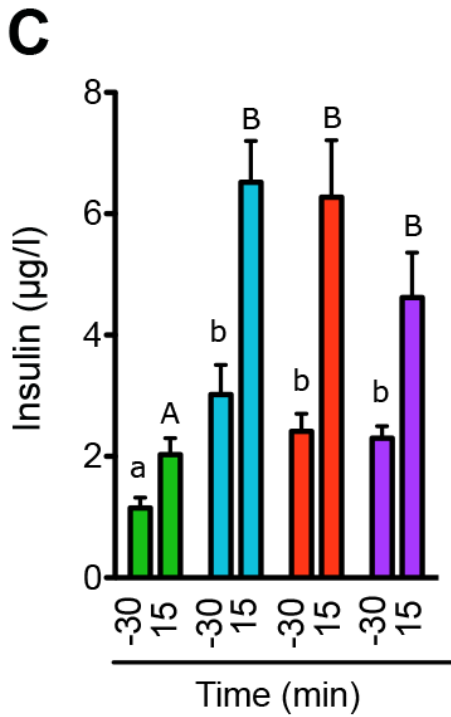
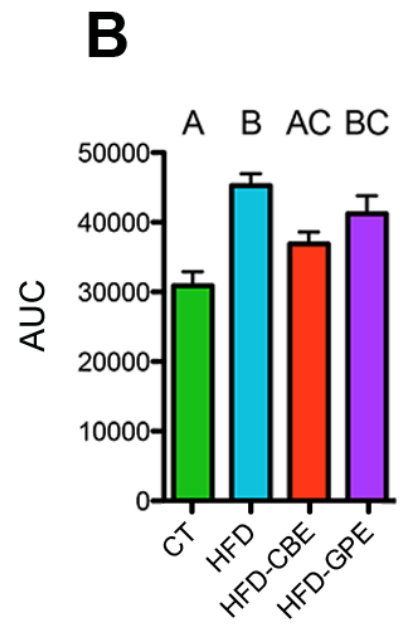
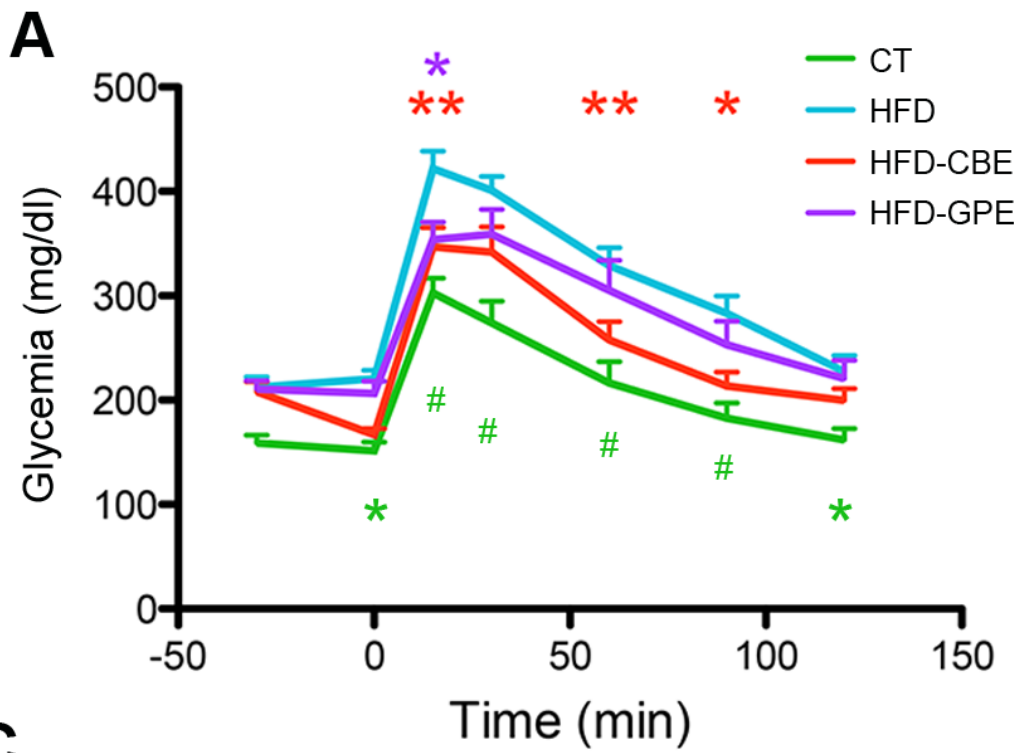
1256 qPCR primer sequences for the targeted mouse genes.

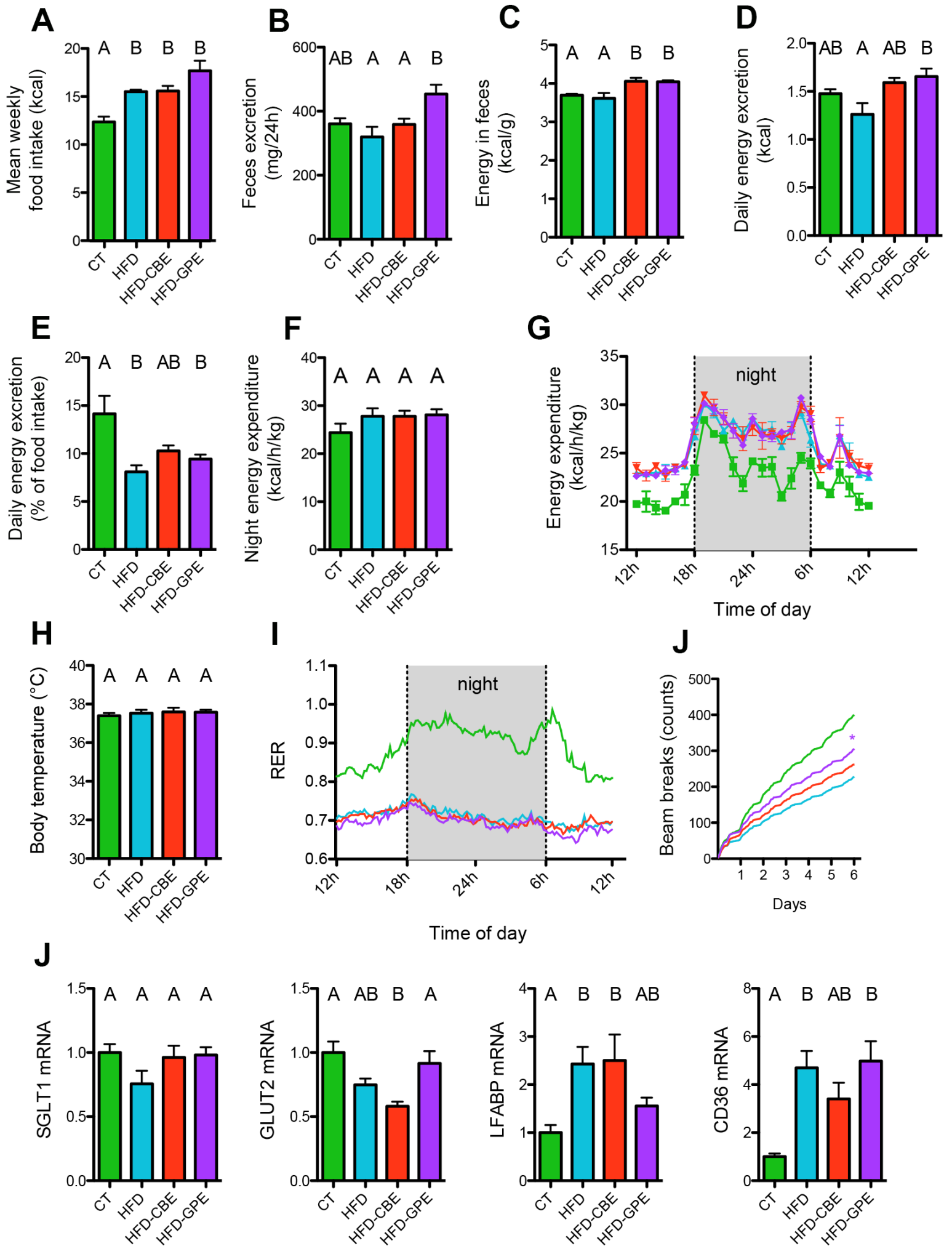
1257

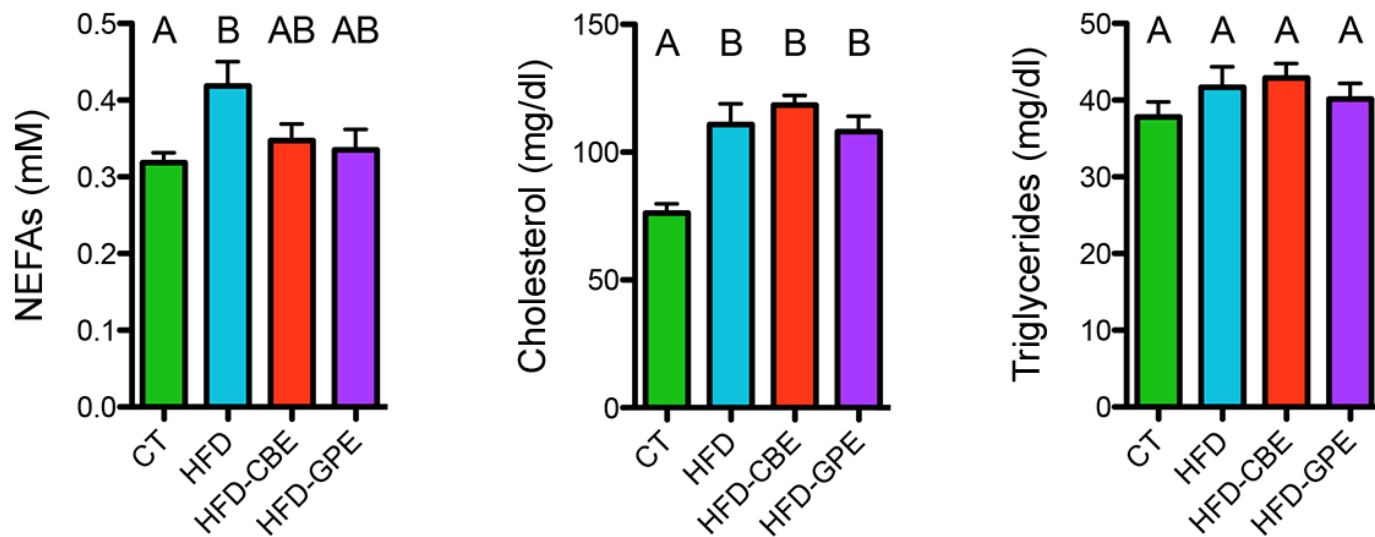
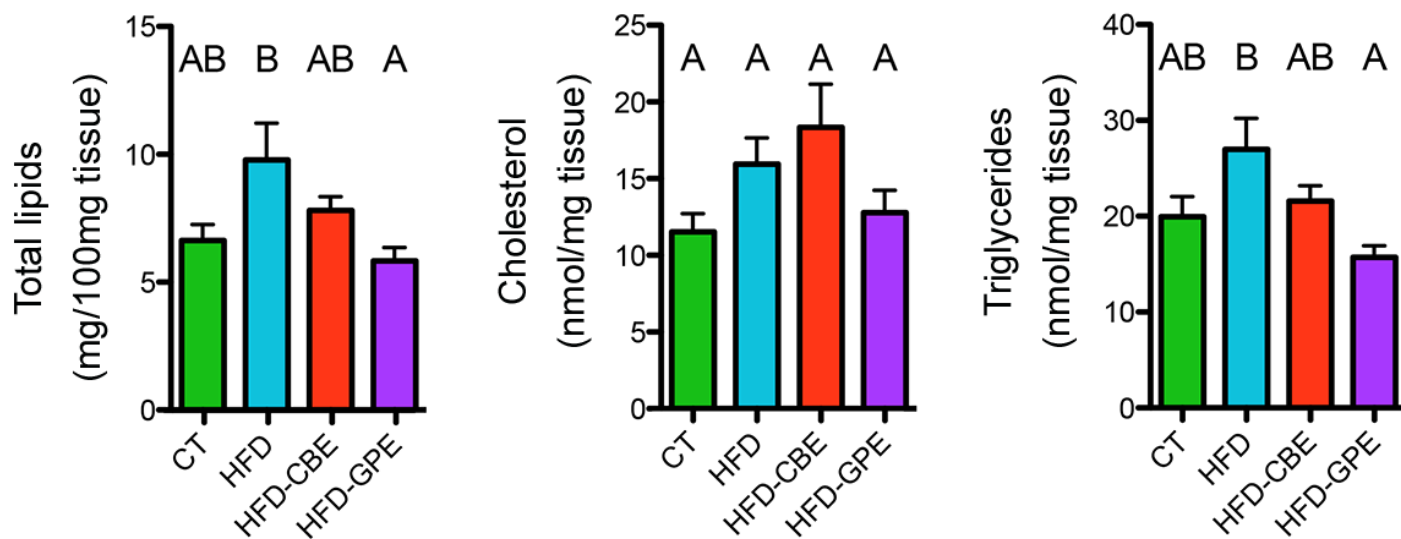
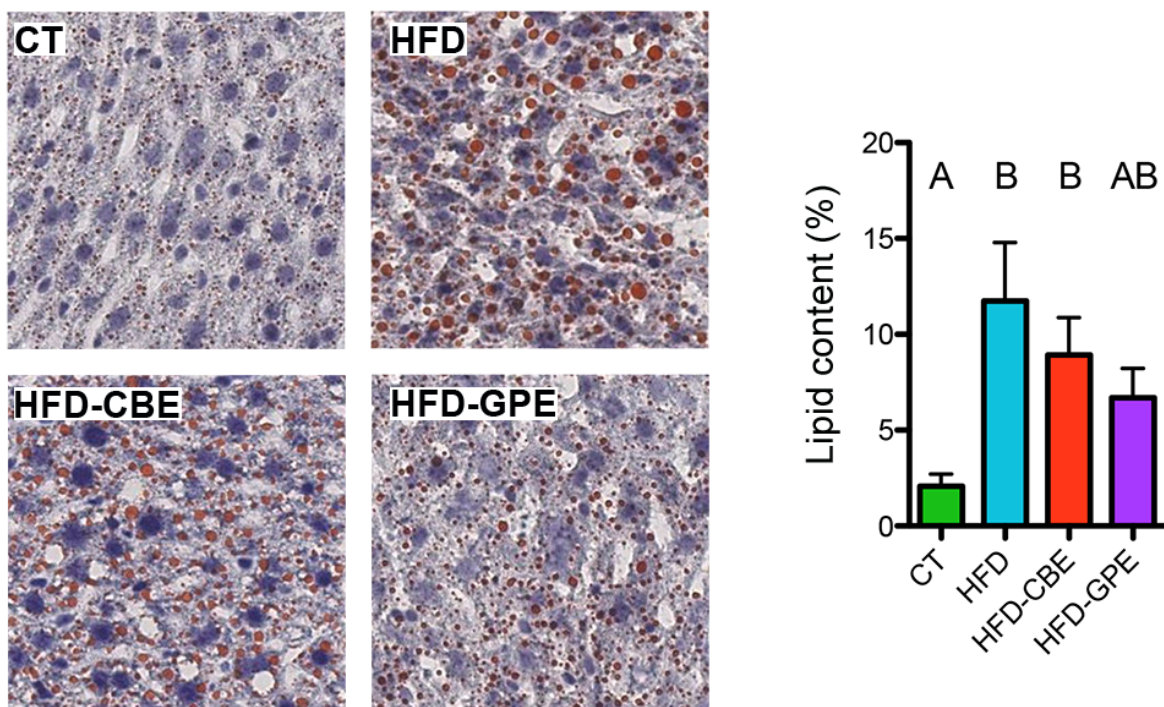
1258 **Table 2**

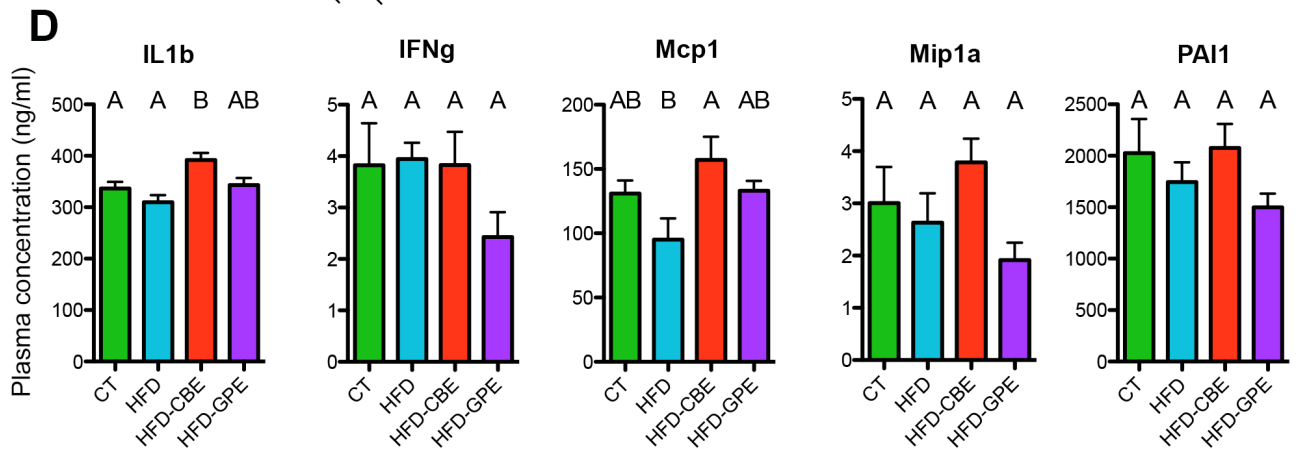
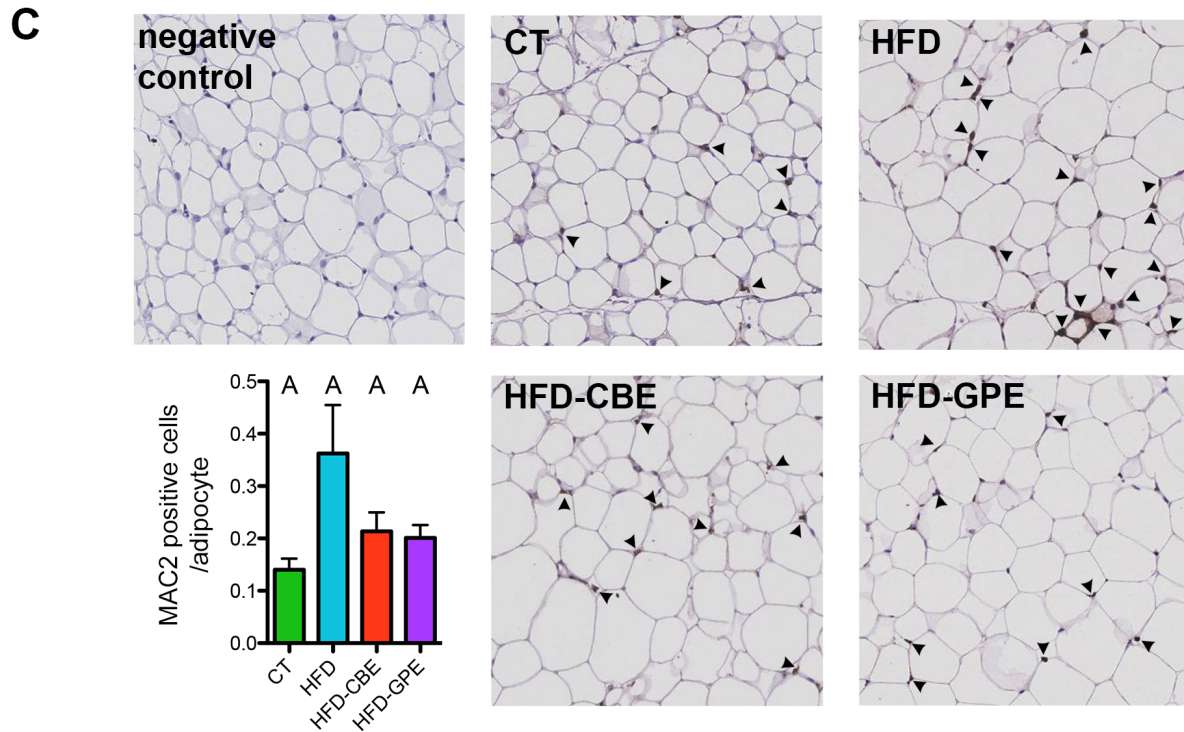
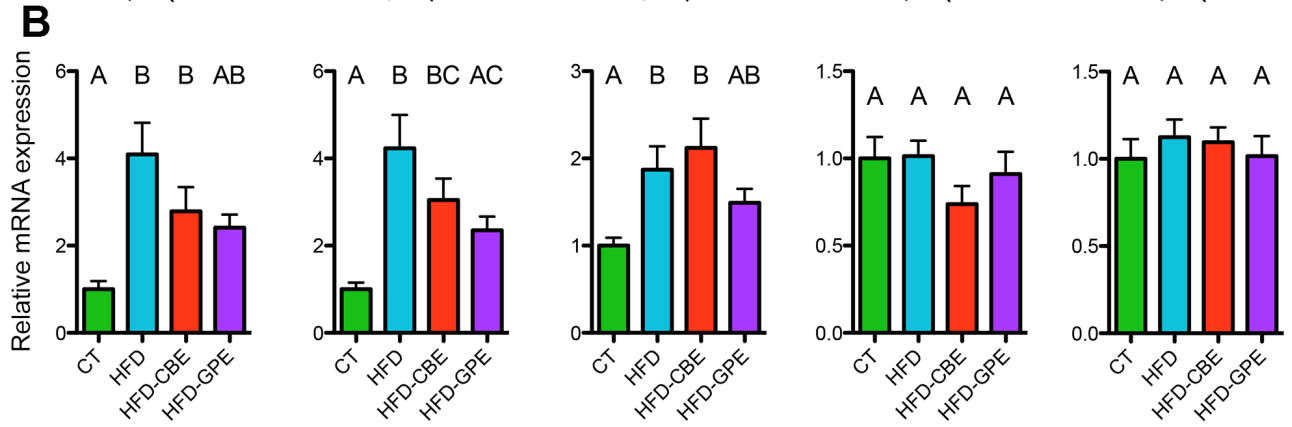
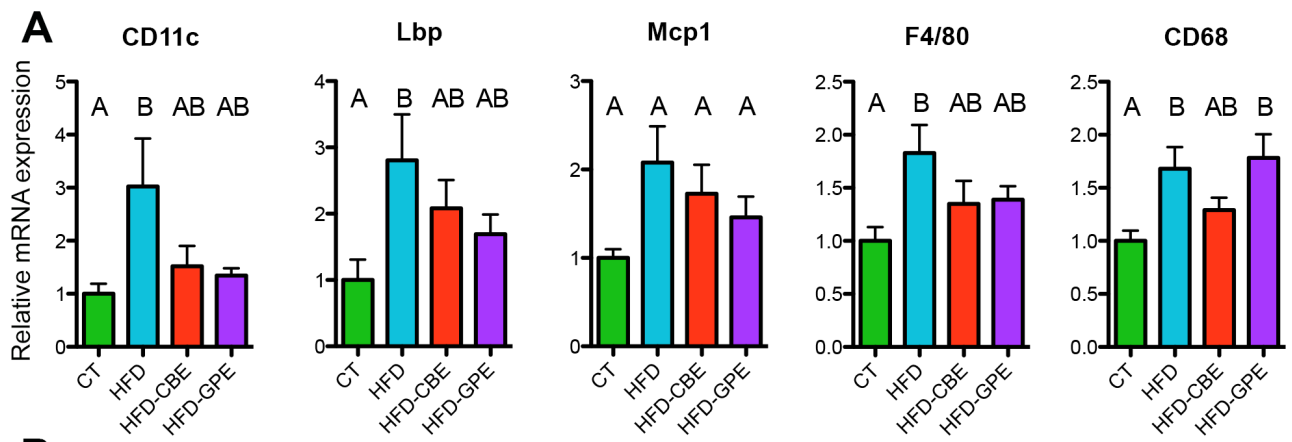
1259 Concentrations of the main components of grape pomace extract and cinnamon
1260 extract.

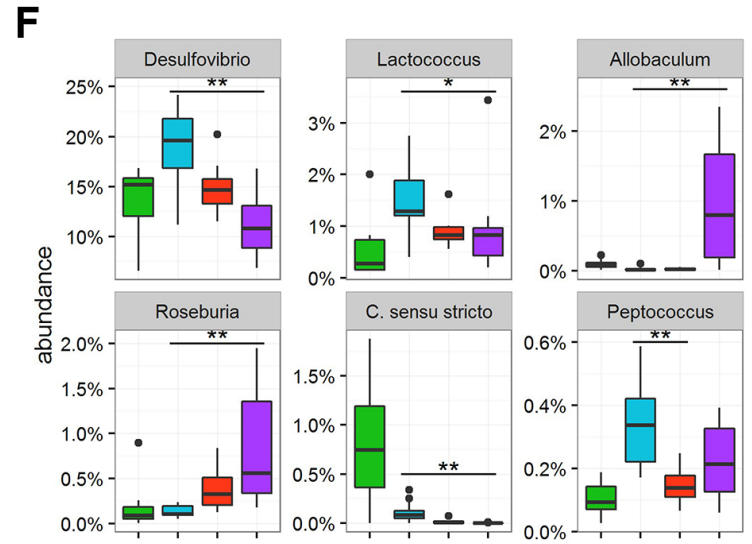
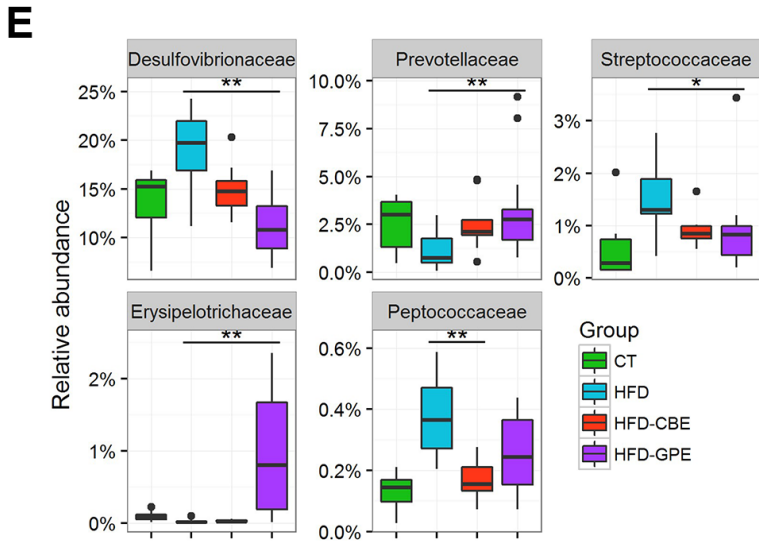
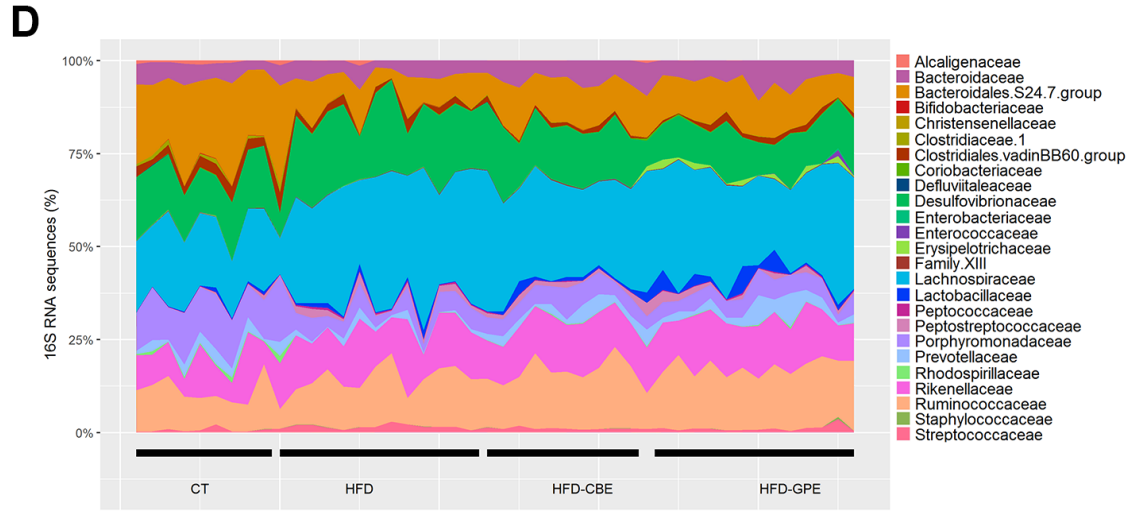
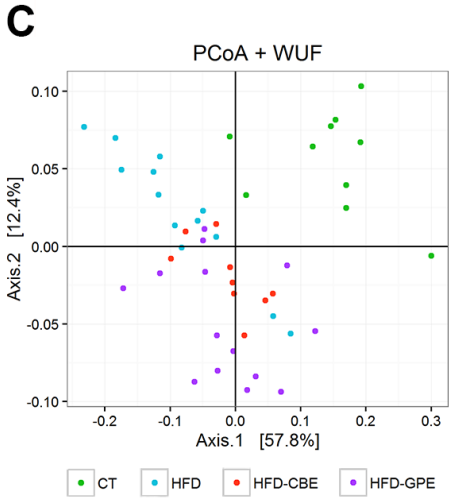
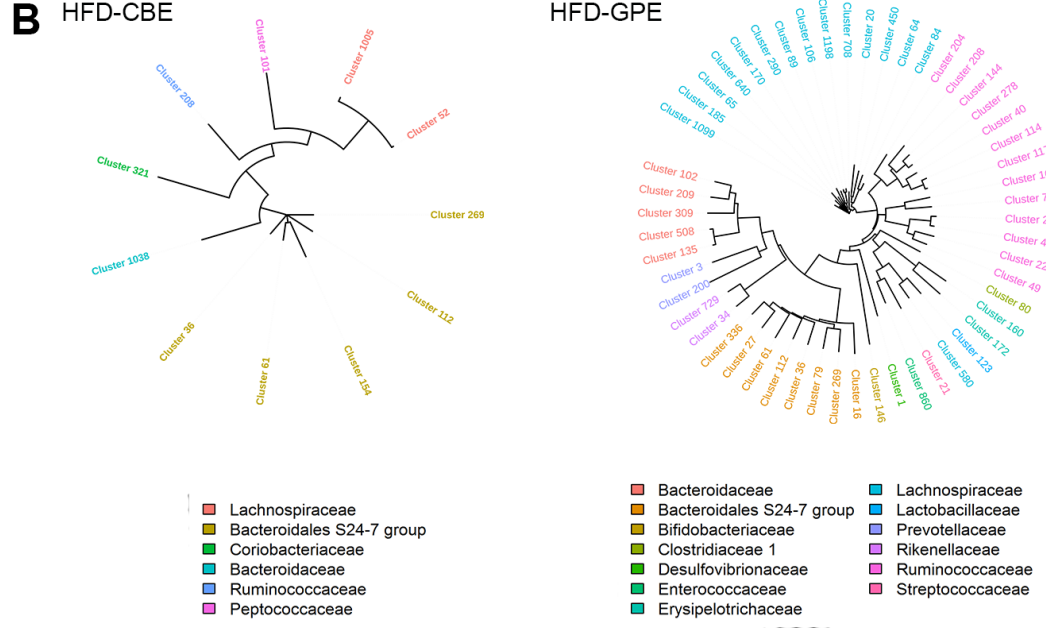


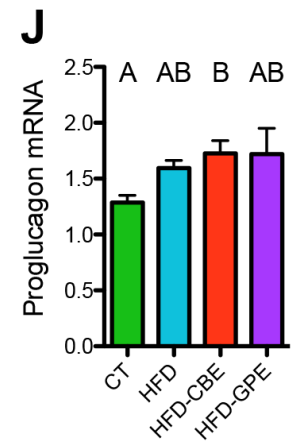
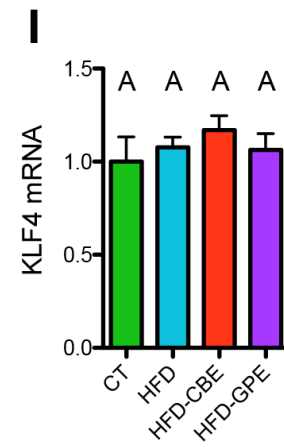
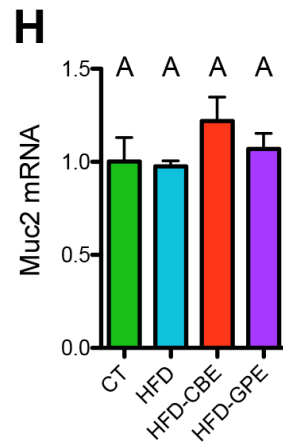
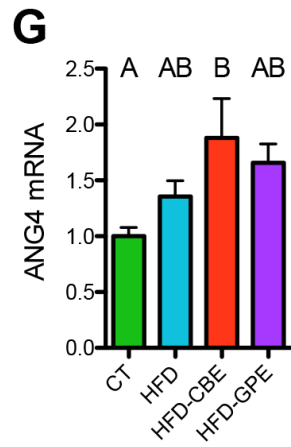
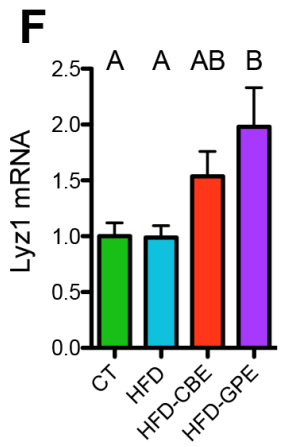
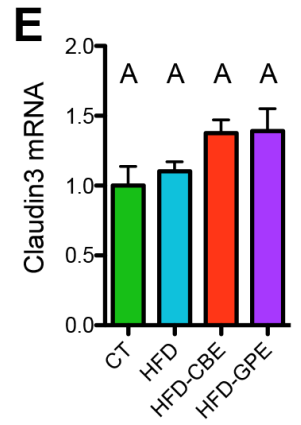
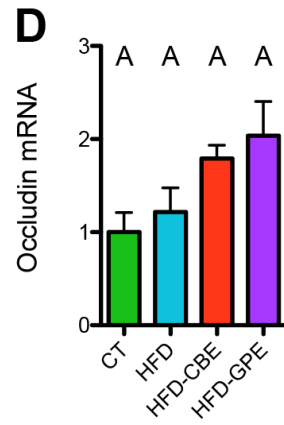
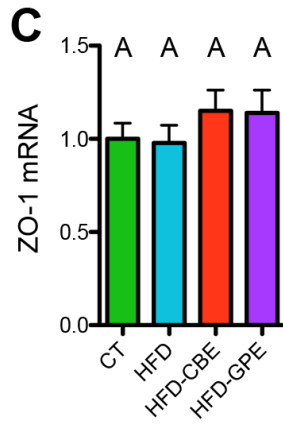
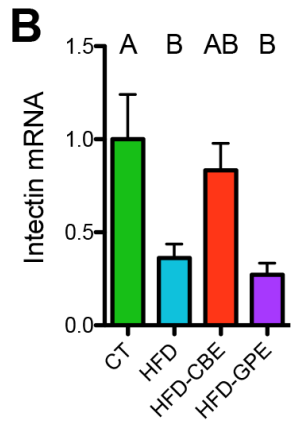
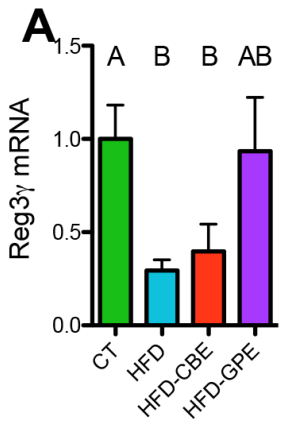




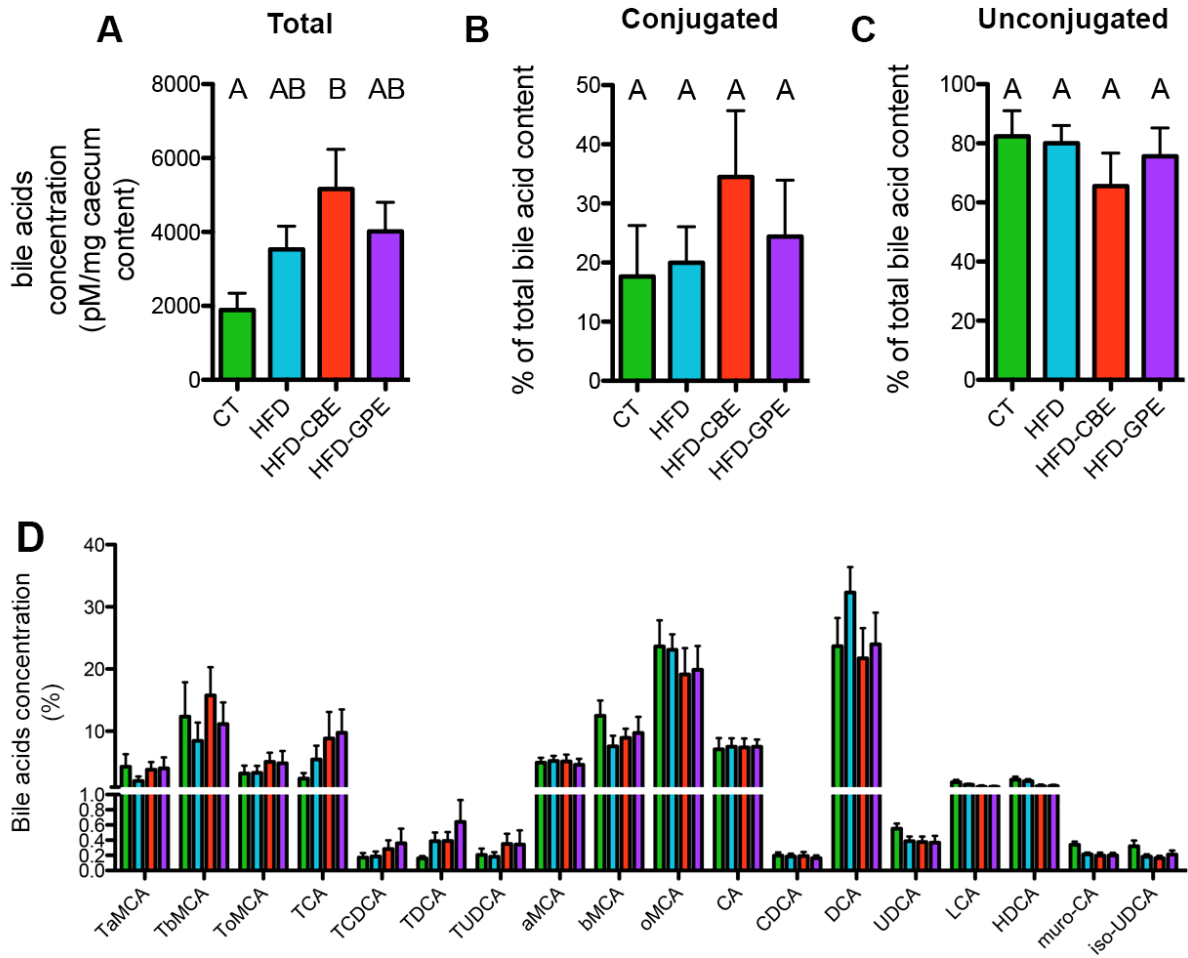
A**B****C**



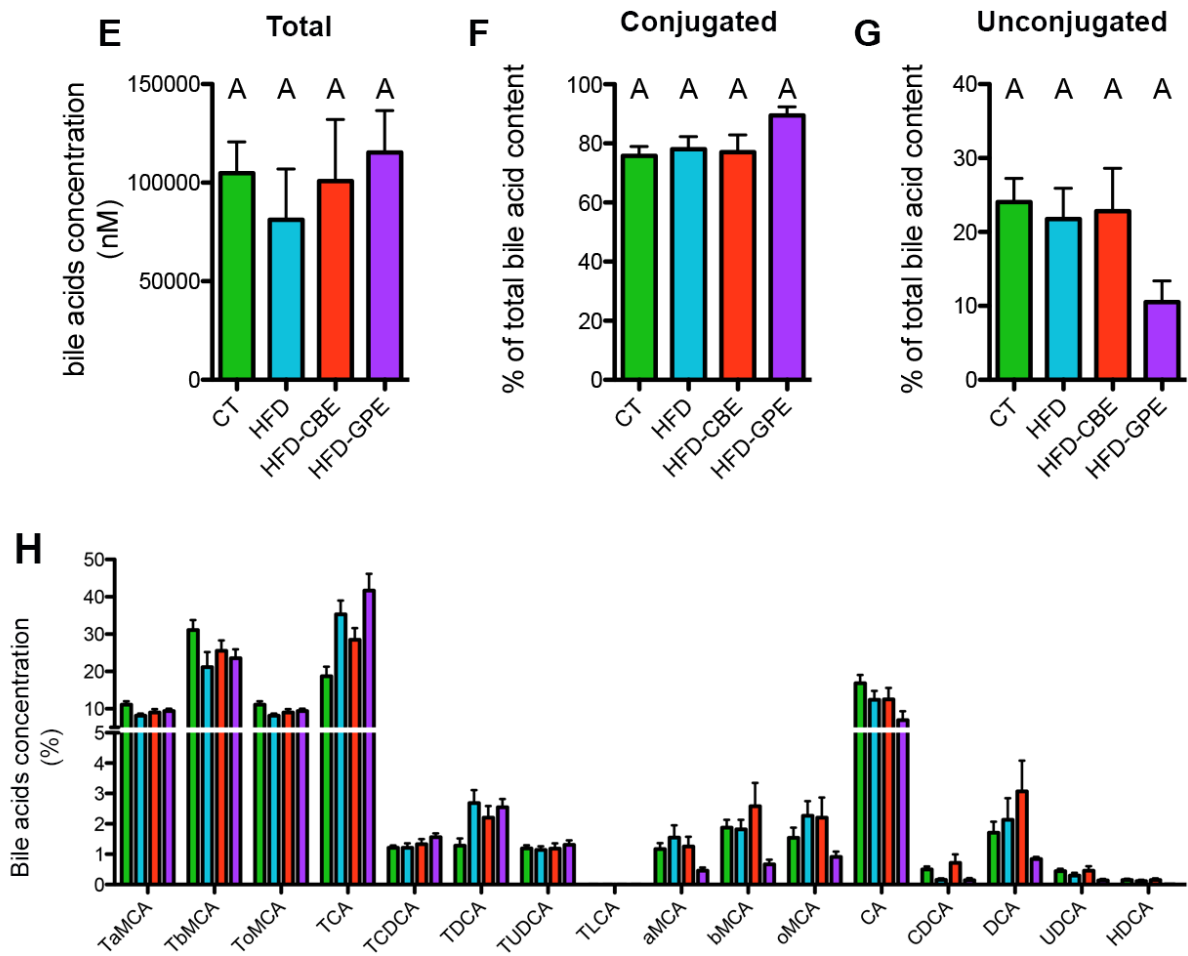


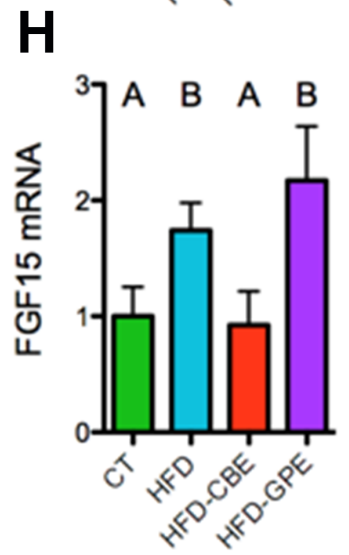
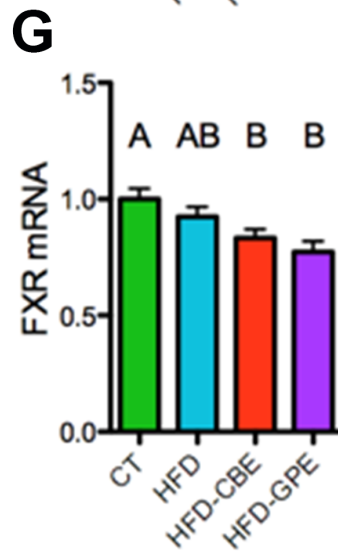
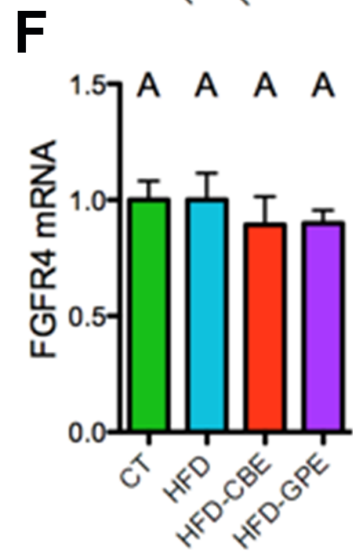
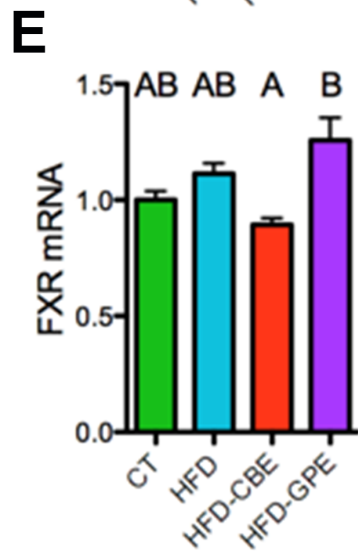
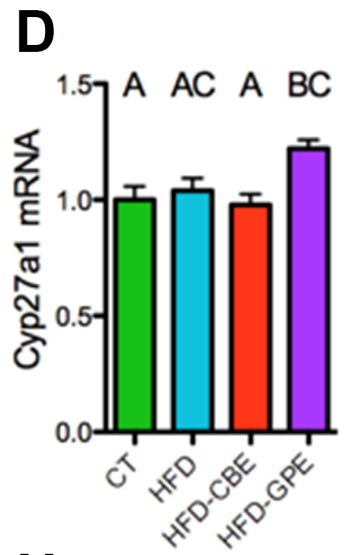
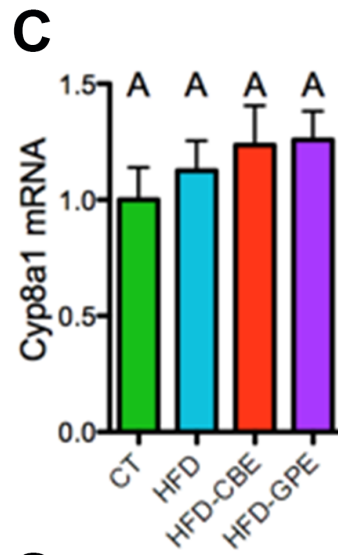
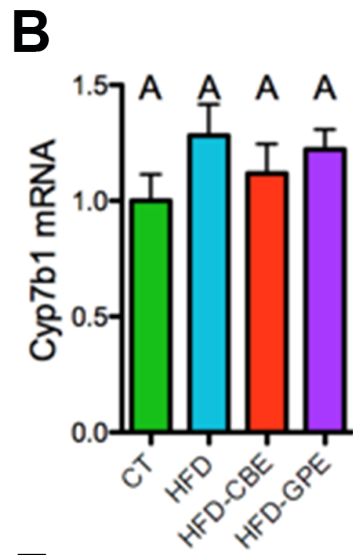
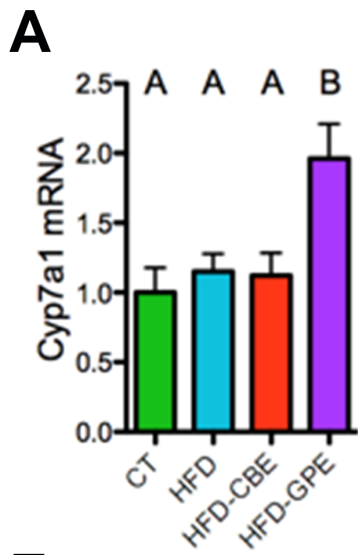


Caecum

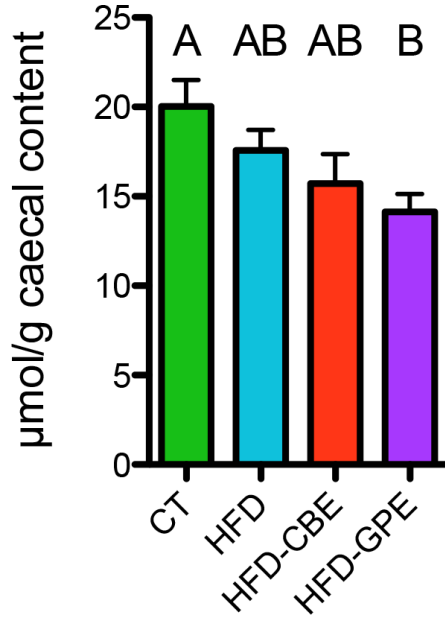


Plasma

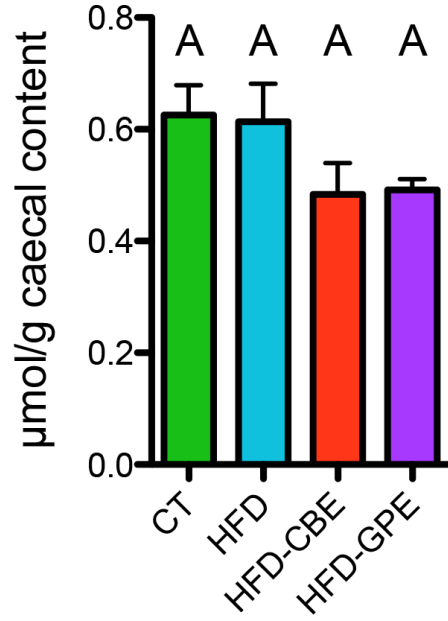




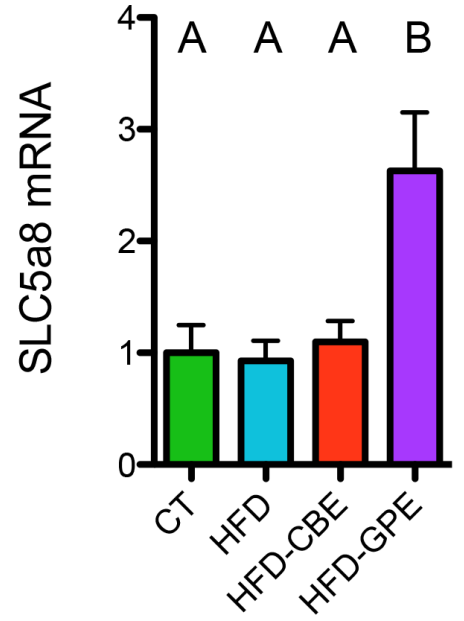
A Total SCFA



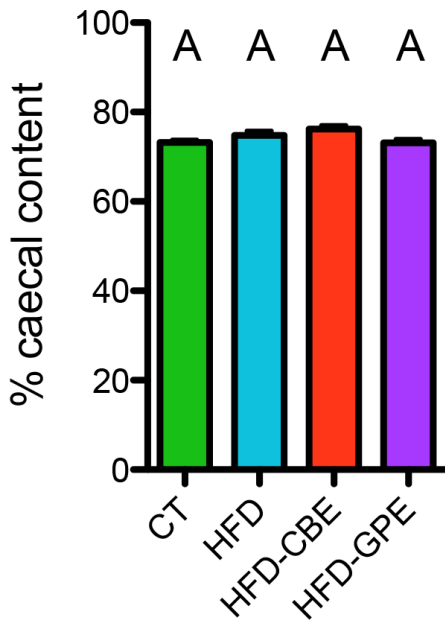
B Iso-SCFA



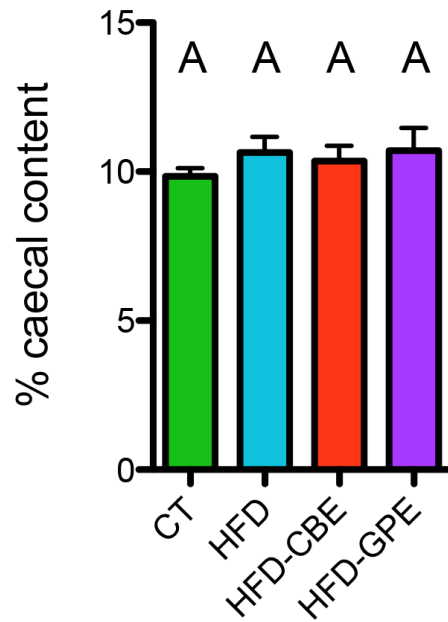
C



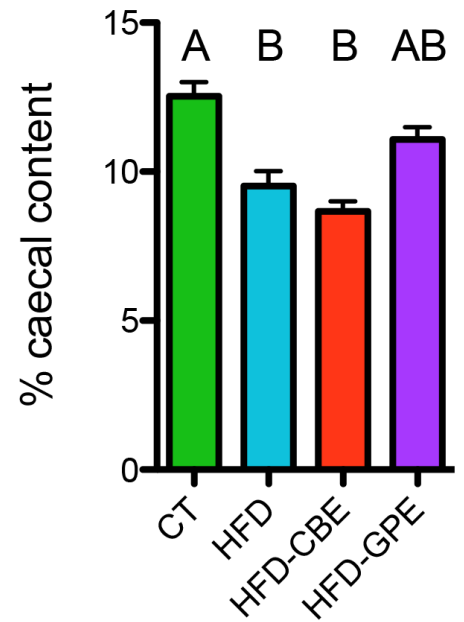
D Acetate



Butyrate



Propionate



Primers	Forward Sequence	Reverse Sequence
Rpl19	GAAGGTCAAAGGGAATGTGTTCA	CCTGTTGCTCACTTGT
Cd11c	ACGTCAGTACAAGGAGATGTTGGA	ATCCTATTGCAGAATGCTTCTTTACC
Mcp1	GCAGTTAACGCCCCACTCA	CCCAGCCTACTCATTGGGATCA
Lbp	GTCCTGGGAATCTGTCCCTG	CCGGTAACCTTGCTGTTGTT
Cd68	CTTCCCACAGGCAGCACAG	AATGATGAGAGGCAGCAAGAGG
F4/80	TGACAACCAGACGGCTTG	GCAGGCGAGGAAAAGATAGTGT
Reg3g	TTCCTGTCCTCCATGATCAAA	CATCCACCTCTGTTGGGTTCC
Intectin	GTTGCCCTGATTCTGCTGG	GCACTATTGCAGAGGTCC-GT
ZO-1	TTTTTGACAGGGGGAGTGG	TGCTGCAGAGGTCAAAGTTCAAG
Occludin	ATGTCCGGCCGATGCTCTC	TTTGGCTGCTCTTGGGTCTGTAT
Claudin3	TCATCGGCAGCAGCATCATCAC	ACGATGGTGATCTTGGCCTTGG
Lyz1	GCCAAGGTCTACAATCGTTGTGAGTTG	CAGTCAGCCAGCTTGACACCACG
Ang 4	CTCTGGCTCAGAATGTAAGGTACGA	GAAATCTTTAAAGGCTCGGTACCC
Muc2	ATGCCACCTCCTCAAAGAC	GTAGTTTCCGTTGGAACAGTGAA
Klf4	AGAGGAGCCCAAGCCAAAGAGG	CCACAGCCGTCACAGTCCAGT
Proglucagon	TGGCAGCACGCCCTTC	GCGCTTCTGTCTGGGA
CYP7a1	GGGATTGCTGTGGTAGTGAGC	GGTATGGAATCAACCCGTTGTC
CYP7b1	TAGGCATGACGATCCTGAAA	TCTCTGGTGAAGTGGACTGAAA
CYP8a1	GATCCGTCGCGGAGATAAGG	CGGGTTGAGGAACCGATCAT
CYP27a1	TCTGGCTACCTGCACTTCTC	GTGTGTTGGATGTCGTGTCC
FXR	TGGGTACCAGGGAGAGACTG	GTGAGCGCGTTGTAGTGGTA
FGFR4	CTCGATCCGCTTTGGGAATTC	CAGGTCTGCCAAATCCTTGTC
FGF15	GAGGACAAAACGAACGAAATT	ACGTCCTTGATGGCAATCG
SGLT1	TCTGTAGTGGCAAGGGGAAG	ACAGGGCTTCTGTGTCTTGG
GLUT2	CTGGGTCTGCAATTTTGCA	TGTAACAGGGTGAAGACCA
LFABP	ACCTCATCCAGAAAGGGAAGG	ACAATGTGCCCAATGTCATG
CD36	GCCAAGCTATTGCGACATGA	ATCTCAATGTCCGAGACTTTTCAAC
SLC5a8	GCATATTCGGCATGGTTGGT	GGGCTCCAATTCCTACCCAT

Comment citer ce document :

Van Hul, M., Geurts, Plovier, Druart, Everard, A., Ståhlman, M., Rhimi, M., Chira, K., Teissedre, P. L., Delzenne, Maguin, E., Guilbot, A., Brochot, A. (Co-dernier auteur), Gérard, P. (Co-dernier auteur), Bäckhed, F. (Co-dernier auteur), Cani, P. D. (Auteur de correspondance) (2018).
Reduced obesity, diabetes and steatosis upon cinnamon and grape pomace are associated with

Table 2. Concentrations of the main components of grape pomace extract and cinnamon extract.

Main tanin concentrations in GPE (mg/g of the extract)		
	mg/g of the extract	Daily dose (ng/d)
Catechin	1.732 ± 0.089	48,40 ± 3,23
Procyanidin B1 dimer	0.100 ± 0.011	2,79 ± 0,18
Procyanidin B2 dimer	0.311 ± 0.032	8,69 ± 0,58
Procyanidin B3 dimer	0.350 ± 0.022	9,78 ± 0,65
Procyanidin B4 dimer	0.090 ± 0.001	2,51 ± 0,16
Procyanidin C2 trimer	0.071 ± 0.001	1,98 ± 0,13
Epicatechin	1.011 ± 0.045	28,25 ± 1,88
Total tanins	3.66 ± 0.625	102,27 ± 6,83
Main anthocyanins concentrations in GPE		
	mg/g of the extract	Daily dose (ng/d)
Delphinidin-3-O-glucoside	1.635 ± 0.016	45,69 ± 3,05
Cyanidin-3-O-glucoside	0.513 ± 0.007	14,33 ± 0,95
Petunidin-3-O-glucoside	2.744 ± 0.027	76,67 ± 5,12
Peonidin-3-O-glucoside	8.687 ± 0.258	242,74 ± 16,21
Malvidin-3-O-glucoside	21.594 ± 0.213	603,39 ± 40,3
Peonidin-3-O-(6'' acetyl-glucoside)	0.546 ± 0.003	15,26 ± 1,02
Malvidin-3-O-(6'' acetyl-glucoside)	1.476 ± 0.026	41,24 ± 2,75
Peonidin-3-O-(6''-p-coumaryl-glucoside)	1.596 ± 0.018	44,6 ± 2,98
Malvidin-3-O-(6''-p-coumaryl-glucoside)	4.624 ± 0.012	129,21 ± 8,63
Total anthocyanins	43.416 ± 6.793	1213,15 ± 81,03
Phenolic composition of GPE		
	mg/g of the extract	Daily dose (ng/d)
Total phenolics (1)	82.663 ± 2.534	2309,81 ± 154,28
Total anthocyanins (2)	43.969 ± 3.497	1228,6 ± 82,06
Total tanins (3)	26.006 ± 1.066	726,67 ± 48,54

(1) Total phenolics, mg/g as gallic acid equivalent (Folin Ciocalteu assay)
(2) Total anthocyanins, mg/g as cyanidin-3-O- glucoside equivalent
(3) Total tanins, mg/g as procyanidin B2 equivalent (Bate-Smith assay)

Main components in CBE		
	mg/g of the extract	Daily dose (ng/d)
Total polyphenols	79	1174,45 ± 40,46
Proanthocyanidin A	90	1337,99 ± 46,09
Coumarin	9	133,8 ± 4,609
Cinnamaldehyde	1,8	26,76 ± 0,92
Eucalyptol	not detected	

Comment citer ce document :

Van Hul, M., Geurts, Plovier, Druart, Everard, A., Ståhlman, M., Rhimi, M., Chira, K., Teissedre, P. L., Delzenne, Maguin, E., Guilbot, A., Brochot, A. (Co-dernier auteur), Gérard, P. (Co-dernier auteur), Bäckhed, F. (Co-dernier auteur), Cani, P. D. (Auteur de correspondance) (2018). Reduced obesity, diabetes and steatosis upon cinnamon and grape pomace are associated with